Journal of Thermal Analysis, Vol. 35 (1989) 2025–2064

Invited Review

THERMODYNAMIC STUDIES OF CLATHRATE HYDRATES*

Osamu Yamamuro and *Hiroshi Suga*

DEPARTMENT OF CHEMISTRY AND CHEMICAL THERMODYNAMICS LABORATORY, FACULTY OF SCIENCE, OSAKA UNIVERSITY, TOYONAKA, OSAKA 560, JAPAN

(Received 21 August, 1988)

Thermodynamic studies of clathrate hydrates, mainly of structures I and II, are considered in this review which is based on 147 references. There are two main subjects. The first is the host lattice energy and the guest-host interaction energy, both of these quantities being related to the enthalpy of dissociation and composition of the hydrates. The second subject concerns orientational ordering phenomena occurring in both host and guest, as reflected in the low temperature heat capacity. The classical theoretical treatment of clathrate formation has been reconsidered on the basis of recent experimental results. Particular emphasis has been given to orientational ordering since this topic is undoubtedly central to clarifying the nature of clathrate hydrates.

1. Introduction

Recently, a number of clathrate compounds have been synthesized and investigated [1]. Some clathrates have already been applied in the industrial field and become important in our life (e.g., cyclodextrin). A clathrate hydrate is one of the most common kinds of clathrate compounds and occurs in nature. The " host" lattice formed by water molecules in a clathrate hydrate incorporates various "guest" molecules of suitable size and shape in well-defined "cages". The history of clathrate hydrates is fairly old; the clathrate hydrate of Cl_2 (called gas hydrate at that time) was found by Davy [2] in 1810.

* Contribution No. 155 from the Chemical Thermodynamics Laboratory.

John Wiley & Sons, Limited, Chichester
Akadémiai Kiadó, Budapest

Nevertheless, the field lay largely dormant until the X-ray diffraction works by Stackelberg and co-workers [3, 4] clarified that gas hydrates are a class of clathrate compounds. These compounds also attract attention as an energy resource because vast deposits of the natural gas (CH_4, C_2H_6, etc.) hydrates were recently found to exist under the ocean bed and the permafrost region [5–7].

Various aspects of clathrate hydrates have been reviewed. Structural studies were reviewed by Jeffrey [8] and NMR, NQR, and dielectric studies were reviewed by Davidson and Ripmeester [9]. Berecz and Balla-Achs [10] published a book "Gas Hydrate" and Makogon [11] "Hydrates of Natural Gas". Ratcliffe and Ripmeester [12] recently reviewed studies concerning molecular disorder in clathrate hydrates. The review by Davidson in 1973 [13] is especially useful and includes almost all studies before 1971. The purpose of the present review is to describe the current state of knowledge on clathrate hydrates from the thermodynamic point of view. Recently, there have been a series of thermodynamic studies providing important knowledge of disorder in clathrate hydrates. It therefore seems to be worthwhile compiling these studies and discussing them on the basis of a new foundation.

The majority of the known clathrate hydrates have one of three types of structure, known as structure I, II, and H, which belong to cubic Pm3n, Fd3m, and hexagonal P6/mmm, respectively. The structure (abbreviated as str. hereafter) H has been found quite recently [14, 15]. Besides the above three, Br_2 [16] and $(CH_3)_2O$ [17] hydrates take the tetragonal $P4_2/mnm$ and $(CH_3)_3CNH_2$ [18] the cubic $I\bar{4}3d$ symmetry. Furthermore, a number of substances including amines and tetra-alkylammonium salts also form clathrate-like or semi-clathrate hydrates; these are not real clathrates because the host and the guest are linked by O—H—N hydrogen-bonds. Recent discovery of enclathration of helium in ice II is one of the hot topics in physics and chemistry of inclusion phenomena [19]. In this review, however, there is not space enough to describe all of these hydrates and so the focus will be on str. I and II. All the host lattices mentioned above, except str. H, are described in detail in the review by Jeffrey [8].

Figure 1 shows the five fundamental cages which constitute the str. I, II, and H hydrates. Circles represent oxygen atoms and bars the hydrogen bonds (protons are omitted in the figure). The structure of the cage is represented by the square bracket notation in which the figures and their indices denote the types of the cage-forming polygons and their numbers in a cage, respectively. The value under the bracket notation is the average geometrical diameter of the cage in pm (1 pm = 0.01 Å). The three host lattices are constructed of combinations of these cages as shown in Table 1, which represent the unit cell structures and the resulting compositions of the hydrate. Each water molecule is coordinated by four neighbouring waters and the hydrogen-bonds constitute the three dimensional network in the crystal as shown in the various ice polymorphs [20]. The O—O

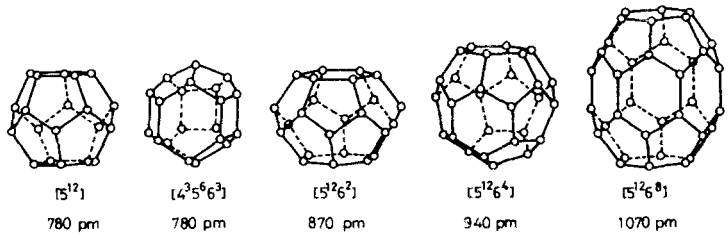

Fig. 1 Five cages constituting the str. I, II, and H. host lattices

Table 1 Unit cell structures of the str. I, II, and H hydrates

		Str. I	Str. II	Str. H
Space group		Pm3n	Fd3m	P6/mmm
Size of unit cell in pm	a	1203	1731	1226
	c	—	—	1017
Water molecule/unit cell		46	136	34
Cages/unit cell	$[5^{12}]$	2	16	3
	$[5^{12}6^2]$	6	0	0
	$[5^{12}6^4]$	0	8	0
	$[4^35^66^3]$	0	0	2
	$[5^{12}6^8]$	0	0	1
Composition space	all cage full	$M \cdot 5(3/4)H_2O$	$M \cdot 5(2/3)H_2O$	—*
	larger cage full	$M \cdot 7(2/3)H_2O$	$M \cdot 17H_2O$	$M \cdot 34H_2O$*

* The str. H is stabilized only when help gas (Xe, H_2S) occupies the smaller two cages.

distances of the bonds are almost the same as that of hexagonal ice Ih but the O—O—O angles differ from the ideal tetrahedral angle, making the empty host lattices unstable relative to ice Ih. Hydrate crystals are formed by stabilization due to the van der Waals interaction between the host and the guest, which overcomes the destabilization due to the strain of the bond angles. The evaluation of the host lattice energy and the guest-host interaction energy is the most important purpose of thermodynamic studies. Such work will be described in detail from both the experimental and theoretical points of view in this review.

Guest species incorporated in the str. I, II, and H are quite varied in size and shape, and the number of them that have been known to be accommodated is more than 120. Table 2 shows the relationship between the largest van der Waals diameter of a typical guest molecule and the structure of the host lattices. The necessary condition for encagement is that the van der Waals diameter of the guest is smaller than the free diameter of the cage, which is roughly calculated by subtracting the van der Waals diameter of oxygen (280 pm) from the geometric cage diameter shown in Table 1. Comparing the free diameter of the larger cage of the three

Table 2 Typical guest molecules arranged in order of the largest van der Waals diameter

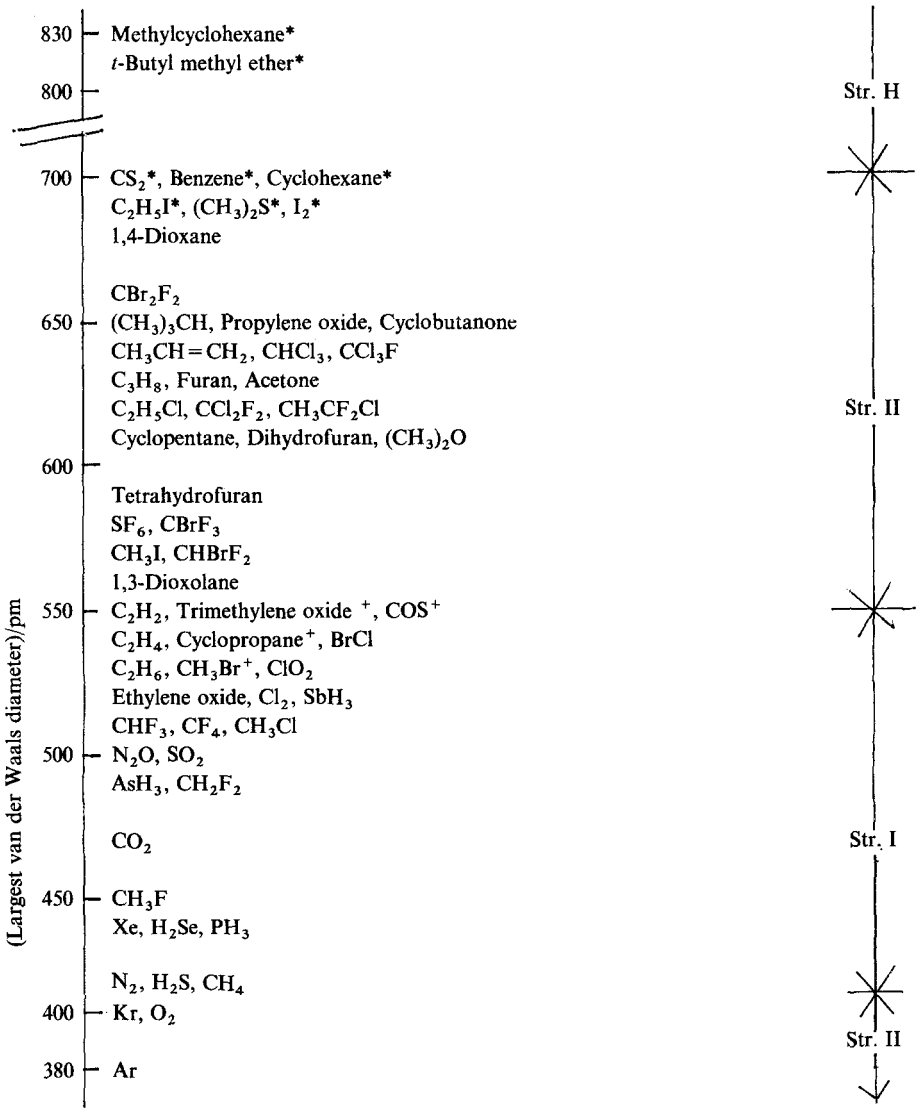

* Stabilized only under the help gas (Xe, H_2S).

\+ Enclathrated both in str. I and II.

structures, it is easily understood that the str. I, II, and H appear in order as the diameter of the guest molecule increases. It is noticeable that the clathrates of the smallest three molecules (Ar, Kr, O_2) exhibit str. II. This was discovered recently and the reason will be discussed in section 5.2.

There are many hydrates incorporating more than one chemical substance as guest species. If the various chemical species enter the cages at random, then the result is called a "mixed hydrate". A "double hydrate" results from the situation with two kinds of guest species where the large guest occupies the larger cages and the small guest the smaller cages. All the str. H hydrates and the str. II hydrates of relatively large (> 680 pm) guest species are double hydrates, in which Xe or H_2S molecules (called "help gas") enter the smaller cages and stabilize the crystal. Details of the mixed and double hydrates have been described in previous reviews [10, 13].

The most characteristic and interesting feature of clathrate hydrates is significant orientational disorder occurring both in the guest and the host. In the host lattice, each water molecule has six possible orientations under the ice condition [21] as in the case of ice Ih, Ic, III, etc. This has been confirmed by the large dielectric constant exceeding 100 [9, 13] and the X-ray [22, 23] and neutron diffraction [24] results showing that two 1/2 protons are located along each hydrogen bond. On the other hand, a guest molecule (except rare gases) exhibits rotational degrees of freedom in the cage and there is, in general, a mismatch between the symmetry of a guest molecule and the site symmetry of the cage center. This results in orientational disorder of the guest molecule. This disorder has been confirmed by dielectric [9, 13], NMR [9, 13], and X-ray and neutron diffraction [22–25] studies, indicating that the nature of the disorder depends on the size and symmetry of the guest molecule and the cage. Thermodynamic studies have not contributed to the investigation of such disorder so far. However, recent heat capacity studies of clathrate hydrates by our group [26–30] have brought a fresh development in the investigation. These studies are the main subject of this review and will be described in detail in chapter 6.

2. Phase diagram

In the preceding chapter, clathrate hydrates were classified on the basis of their crystal structures. Another important classification based on phase diagrams is presented here.

The phase diagrams of clathrate hydrate systems are divided broadly into two groups depending on the solubility of the guest species in water: water-insoluble species (*i*-type) and water-soluble species (*s*-type). Figure 2, based on Sortland's work [31] on the str. II SF_6 hydrate, is a typical $p-T$ phase plane of an *i*-type phase diagram. The hydrate is stable in the low-temperature and high-pressure region surrounded by the H–I–G, H–L_1–G, and H–L_1–L_2 phase equilibrium lines. Here H stands for the hydrate, I for ice Ih, G for the guest gas, and L_1 and L_2 for the liquid

phases rich in water and the guest species, respectively. There are two invariant quadruple points Q_1 and Q_2. This type of phase diagram is further labelled i_2 after these two invariant points. For light gases such as rare gases, N_2, O_2, and CH_4, the H–L_2–G equilibrium line terminates at a critical point before it intersects the H–L_1–G line. This type of phase diagram is labelled i_1 corresponding to only one quadruple point Q_1. Cyclopropane · nH_2O is a rare hydrate which takes either the structure I or II, depending on pressure and temperature. Figure 3 shows the $p-T$ phase diagram of the cyclopropane–H_2O system determined by Hafemann and Miller [32] and Majid et al. [33]. This diagram has four quadruple points.

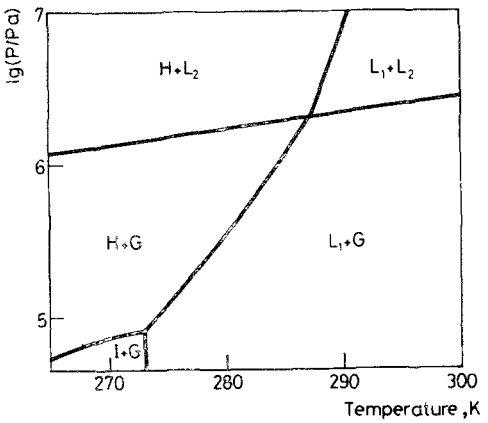

Fig. 2 $p-T$ phase diagram of i_2-type (SF_6–H_2O) system (Ref. [31])

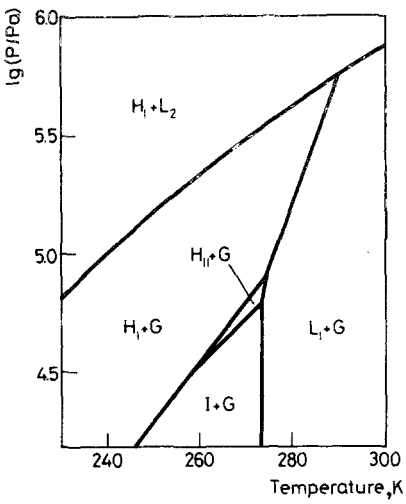

Fig. 3 $p-T$ phase diagram of i_4-type (cyclopropane–H_2O) system (Ref. [32])

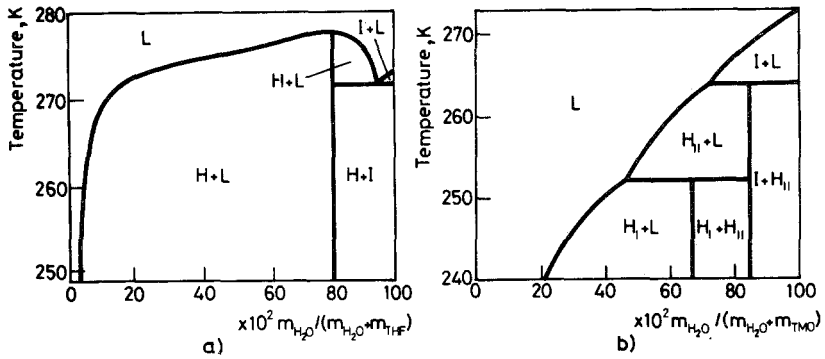

Fig. 4 $x-T$ diagram of (a) s_c-type (THF–H_2O) system (Ref. [34]) and (b) s_i-type (TMO–H_2O) system (Ref. [35])

When the guest species are soluble in water, there is only one liquid phase and Q_2 is absent. When Q_2 is replaced by congruent or incongruent melting points, the phase diagrams are labelled s_c and s_i, respectively. Some cyclic ethers and ketones whose van der Waals diameters are smaller than 180 pm belong to these groups. These guest species are usually in the liquid state at atmospheric pressure and so their phase diagrams are most conveniently shown in the temperature and composition projection at atmospheric pressure. Figures 4a and 4b show the s_c-type phase diagram of tetrahydrofuran (THF) hydrate determined by Callanan and Sloan [34], and the s_i-type phase diagram of trimethylene oxide hydrate by Rosso and Carbonnel [35]. The former exhibits str. II hydrate and the latter both str. I and II depending on the composition of the solution.

For the *i*-type hydrate, it is quite difficult to determine the phase boundary lines, especially the H–I–G line. This is because the formation and decomposition processes of clathrate hydrates take place slowly only at the interface between ice (or water) and the gas. This problem has been overcome to some extent by the method developed by Barrer and Edge [36]. They observed the formation process of Ar, Kr, and Xe hydrates while grinding the crystals by rolling steel ball-bearings over them. For the *s*-type phase diagram, on the other hand, one can easily determine the phase boundaries by usual thermal analysis techniques at atmospheric pressure for samples having various compositions.

Table 3 lists, for each type of phase diagram, typical guest species, structure, and temperature and pressure at Q_1 and Q_2. For the *i*-type hydrates, this table is substantially the same as Table 1 in the review [13], although several new references have been included. For the *s*-type hydrates, however, some hydrates found after 1971 were not previously tabulated and the values of Q_1 and Q_2 have been improved by more reliable experiments.

Table 3 Classification of typical hydrates based on $p-T$ phase diagram

Type	Guest species	Str.	T, K	P, MPa	T, K	P, MPa	Ref.
			at Q_1		at Q_2		
	Ar	II	272.4	8.8	—		36, 37
	Kr	II	273.1	1.45	—		36, 38
	Xe	I	273.2	0.15	—		3, 36, 39
i_1	N_2	I	271.9	14.34	—		37,40
	O_2	II	272.2	11.06	—		40
	CH_4	I	273.0	2.56	—		41,42, 43, 44
	C_2H_4	I	273.1	0.551	—		45, 46, 47
	Cl_2	I	272.9	0.0320	301.5,	0.85	4, 48, 49, 50
	CO_2	I	273.2	1.26	283.1,	4.50	4, 51, 52
	N_2O	I	273.2	0.98	285 ,	4.2	53
	H_2S	I	272.8	0.0930	302.7,	2.24	54, 55, 56, 57
i_2	SO_2	I	270.6	0.0278	285.3,	0.236	58, 59, 60
	SF_6	II	273.2	0.081	287.2,	2.02	31,61
	C_2H_6	I	273.1	0.530	287.9,	3.39	41, 43, 46, 62, 63, 64
	C_3H_8	II	273.2	0.176	278.9,	0.552	42, 43, 45, 51, 65, 66
	CH_3Cl	II	273.2	0.042	293.7,	0.50	67
i_4	Cyclopropane	I	—		289.4,	0.566	32, 33
		II	273.1	0.0627	—		
	Ethylene oxide	I	271.1		284.11 ± 0.02		29, 34, 68, 69, 70, 71
	Propylene oxide	II	268.5		268.6		72, 73, 74, 75
	Tetrahydrofuran	II	272.2		277.5 ± 0.1		27, 34, 71, 76, 77, 78
s_c*	2,5-Dihydrofuran	II	269.9		272.0		74,75, 79
	Cyclobutanone	II	?		273.2		80
	1,3-Dioxolane	II	?		270.5		74, 75, 81, 82
	1,3-Dioxane	II	?		269.6		74, 82, 83
	Trimethylene oxide	I	—		252.4		75, 85
		II	—		260.1		75, 85
s_i+	Acetone	II	—		253.4		77, 85
	1,4-Dioxane	II	—		260		83, 86
	Isoxazole	II	—		271		87
	Isothiazole	II	—		271		88

* Q_1 corresponds to the eutectic temperature between ice and the hydrate and Q_2 the congruent temperature of the hydrate.

+ Q_2 corresponds to the peritectic temperature.

3. Enthalpy of dissociation

Enthalpy of dissociation is one of the most important thermodynamic values, from which the guest-water interaction energy and the energy of the host water lattice can be derived with the help of the ideal solution theory described later. The experimental technique to obtain the enthalpy of dissociation and the results for some typical hydrates are given here.

For hydrates having the *i*-type phase diagram, the enthalpy of dissociation can be obtained from either of the two reactions:

$$M \cdot nH_2O(cr) = nH_2O(cr) + M(g), \quad (1)$$

$$M \cdot nH_2O(cr) = nH_2O(l) + M(g), \quad (2)$$

where M stands for guest molecule.

In the past, the enthalpy of dissociation has generally been obtained by applying the Clausius–Clapeyron equation to the dependence of $\ln p$ on $1/T$ along the H–I–G and H–L_1–G curves. Accurate application of the method requires the correction of the resulting enthalpies for nonideality of the gas and solubility of M in liquid water. The enthalpy of dissociation obtained by this method is compiled in the previous review [13].

Recently, Handa [89] developed a calorimetric technique which directly and simultaneously determines the enthalpy of dissociation, composition, and heat capacity of the *i*-type hydrates. He combined a Tian–Calvet heat-flow calorimeter with a fixed-volume vessel, the inside pressure of which was measured with a transducer. A hydrate sample prepared outside the calorimeter was loaded into the sample cell in a liquid nitrogen bath whose temperature was low enough to suppress decomposition. Then the cell was installed in the calorimeter which had already been cooled down to liquid nitrogen temperature. The first step was to make a C_p measurement in order to check the amount of unreacted ice using a guest-pressure which was higher than the dissociation pressure of the hydrate. Next, the hydrate was allowed to dissociate on heating under the guest-pressure which was, in this case, lower than the dissociation pressure. During the second run, the pressure of the guest expanding into the vessel was measured simultaneously with the thermopile signal. The composition of the hydrate was determined from the final pressure and the enthalpy of dissociation was calculated by integration of the thermopile signal.

Table 4 shows the enthalpies of dissociation of the six important hydrates of light gases (Xe, Kr, CH_4, C_2H_6, C_3H_8, and $(CH_3)_3CH$), which have been compiled by Handa [89, 90]. All the values have been corrected to the values at the standard state (273.15 K and 101325 Pa) using the following data: the C_p difference between the

Table 4 Molar enthalpy of dissociation of light gas hydrates $M \cdot nH_2O$ at the standard state (101 325 Pa, 273.15 K) (from Ref. [89] and [90]

Guest	Str.	$\Delta H_m(H \rightarrow I+G)$, kJ mol^{-1}	$\Delta H_m(H \rightarrow W+G)$, kJ mol^{-1}	Method	Ref.
		19.54 ± 0.24	56.20 ± 0.25	direct	89
Kr	II	—	58.2	P_{diss}	3
		—	56.3*	P_{diss}	38
		20.5	—	P_{diss}	36
		26.50 ± 0.17	61.96 ± 0.19	direct	89
		25.79 ± 0.41	61.67 ± 0. 84	P_{diss}	91
Xe	I	—	69.2	P_{diss}	39
		—	69.9	P_{diss}	3
		—	64.0$^+$	P_{diss}	92
		24.0	—	P_{diss}	36
		18.13 ± 0.27	54.19 ± 0.28	direct	90
		23.37	67.85	P_{diss}	93
		—	54.36	P_{diss}	62
CH_4	I	—	55.12	P_{diss}	94
		—	55.07	P_{diss}	95
		—	53.41	P_{diss}	37
		19.06	—	P_{diss}	96
		25.70 ± 0.37	71.80 ± 0.38	direct	90
		23.75	69.71	P_{diss}	62
C_2H_6	II	—	73.88	P_{diss}	94
		—	86.32	P_{diss}	45
		—	76.09	P_{diss}	97
		27.00 ± 0.33	129.2 ± 0.4	direct	90
		27.91	126.9	P_{diss}	96
C_3H_8	II	—	109.1	P_{diss}	45
		28.30	—	P_{diss}	98
		26.68	—	P_{diss}	99

* n = 6.1 was assumed by the author in Ref. [38].

$^+$ n = 6.0 was assumed by the author in Ref. [92].

hydrate and ice, the molar volumes of the hydrate, ice, and water, the solubility of the guest gas in water and their standard state function for the solution process, and the fugacity of the guest gas. There are large discrepancies in the values previously determined by phase equilibrium studies. This is considered to be mainly due to the errors in the phase diagrams themselves and the use of the Clausius–Clapeyron equation which leads to compounding of errors. The values determined by the direct method are much more reliable.

Table 5 Molar enthalpy of congruent melting and dissociation at the standard state (101 325 Pa, 273.15 K) of the s_c-type hydrates

Guest species	Str.	$\Delta H_m(H \rightarrow \text{solution})$, kJ mol^{-1}	$\Delta H_m(H \rightarrow W+G)$, kJ mol^{-1}	Method	Ref.
Ethylene oxide	I	48 ± 1	75 ± 2	Calvet	71
		49.4	—	DSC	34
		48.26	—	Adiabatic	29
Propylene oxide	II	92.7	134 ± 1	Calvet	74
Tetrahydrofuran	II	98 ± 2	139 ± 4	Calvet	71
		98.8 ± 0.7	—	DSC	34
		99.1	143 ± 1	Calvet	74
		96.98	—	Adiabatic	27
2,5-Dihydrofuran	II	92.9	—	Calvet	74
1,3-Dioxolane	II	99.1	140 ± 1	Calvet	74
1,3-Dioxane	II	89.9	135.1	Calvet	74

For the hydrates having the s_c-type phase diagram, the enthalpy of congruent melting (H $\rightarrow$solution) is measured at atmospheric pressure in place of the enthalpy of dissociation (H $\rightarrow$I + G). The third column of Table 5 shows the molar enthalpies of congruent melting $\Delta_{fus}H_m$ of several cyclic ethers. For all the hydrates, the values determined by the different calorimetric techniques coincide with each other within their experimental errors. Thus, enthalpy of congruent melting is much easier to determine than enthalpy of dissociation. The fourth column shows the enthalpies of dissociation at the standard state, which were calculated from the enthalpies of congruent melting using the following data: the enthalpy of vaporization of the guest, the differences in heat capacities between the ideal gas and liquid, and between the solution and the hydrate, and the enthalpy of melting at 273.15 K.

For the s_i-type hydrates, the enthalpy of the process (H $\rightarrow$solution) is known only for 1,4-dioxane, on the basis of DSC measurement by Nakayama et al. [86]. These workers obtained an enthalpy in the range 51.3–55.6 kJ mol^{-1} which corresponds to an uncertainty of composition dioxane·$36H_2O$ to dioxane·$39H_2O$.

The enthalpy of dissociation reflects the magnitude of the stabilization due to the van der Waals interaction between the host and the guest. It is reasonable that the experimental values in Tables 4 and 5 increase as the size of guest molecules increases. Such a discussion will be performed quantitatively in chapter 5.

4. Composition of hydrates

If clathrate hydrates are stoichiometric compounds and all the cages are occupied by guest species, the composition of the hydrates becomes the unique values given in Table 2. However, the clathrate hydrates are a kind of non-stoichiometric compound whose composition changes depending on the guest-pressure and temperature. In this chapter, experimental methods to determine the compositions of clathrate hydrates and the typical results are presented.

A classical method to obtain the compositions of the *i*-type hydrates is from a knowledge of the enthalpies of the reactions (1) and (2) which are determined from the phase equilibria with the help of the Clausius–Clapeyron equation. The difference between both enthalpies is merely the enthalpy of fusion for n moles of ice. This method is an indirect one which uses secondary data (enthalpies of dissociation) and so frequently leads large accumulation of errors.

A more sophisticated method to determine the composition of the *i*-type hydrates was developed by Miller and Strong [100]. They utilized the lowering effect on the activity of water by adding solute (usually NaCl) and consequent increase of the dissociation pressure of the hydrates. At a constant temperature, the equilibrium constant of the reaction (2) can be assumed to be unaffected by adding solute and so

$$n = \frac{\ln [p_M(S)/p_M(0)]}{\ln [a_W(0)/a_W(S)]}, \tag{3}$$

where $p_M(S)$ and $p_M(0)$ are the equilibrium partial pressure (exactly fugacity) of M in the presence and absence of the solute, $a_w(S)$ and $a_w(0)$ the corresponding activities of water. When the composition is not affected by the presence of the solute, this method is strictly valid. Otherwise, one should obtain the dependence of n on the concentration of the solute and extrapolate it to the infinite dilution limit.

Direct measurements were carried out for several *i*-type hydrates by Barrer and Edge [36] and by Handa [89, 90]. The former measured the amount of Ar, Kr, and Xe gases consumed at the reactions between the respective guests and ice. The latter, on the other hand, measured the amount of Xe, Kr, CH_4, C_2H_6, and C_3H_8 gases released at the decomposition of each hydrate. Both the measurements were carried out at lower temperatures than Q_1. Successful application of these direct methods depends either on the complete reaction of the hydrate or the accurate estimation of the unreacted ice. Handa [89, 90] checked the presence of remaining H_2O by observing the melting of ice in the manner described in the last section. The greatest merit of the direct method is that it can determine the composition of the hydrate which is formed not only at the Q_1 or on the H–I–L_1 line but also at any point in the hydrate-stable region on the $p-T$ plane.

Determination of the composition of the s_c-type hydrate is substantially the same

as that of the phase diagram. If the prepared solution has just the composition of the hydrate, no eutectic but only congruent melting should be observed. The composition is also accurately determined by the comparison of measured hydrate density with X-ray lattice parameter [3]. The compositions of tetrahydrofuran and chloroform hydrates were determined from the measurements of volume change at decomposition and the density of the resulting solution [101]. For the s_i-type hydrates, determination of the composition at the peritectic point is generally not easy owing to the slowness of the peritectic decomposition process.

Table 6 gives the composition of typical hydrates (hydration number n in the formula $M \cdot nH_2O$). The tabulated i-type hydrates were formed at Q_1 in the phase equilibrium method, and at a little higher temperature than Q_1 in the NaCl method. The conditions where the i-type hydrates were formed in the direct method are described in the fourth column of the table. The tabulated s-type hydrates were formed at atmospheric pressure.

Table 6 Composition ($M \cdot nH_2O$) of typical clathrate hydrates

Guest species	Str.	n	Method	Ref.
Ar	II	6.15	phase equil.	36, 37
		6.0	direct (90–149 K, P_{diss})	36
Kr	II	6.90	phase equil.	3, 36
		6.0	direct (150–203 K, 2.7 MPa)	36
		6.10	direct (253 K, 2.7 MPa)	89
		5.99	direct (273 K, 8.0 MPa)	30
Xe	I	7.61	phase equil.	3, 36
		6.0	direct (211–268 K, P_{diss})	36
		6.0	phase equil.	91
		5.9	direct (253 K, 2.0 MPa)	89
		6.29	direct (273.15 K, 0.155 MPa)	102
		6.18	direct (273 K, 2.9 MPa)	30
N_2	I	6.01	phase equil.	40
		6.21	NaCl	103
O_2	II	6.06	phase equil.	40
		6.11	NaCl	103
Cl_2	I	7.05	phase equil.	48
		6.90	NaCl	48
CO_2	I	6.07	phase equil.	52
H_2S	I	6.06	phase equil.	56
SO_2	I	6.20	phase equil.	3
		6.0	vol. change	59

Table 6 (continued)

Guest species	Str.	n	Method	Ref.
SF_6	II	17.02	phase equil.	31
CH_4	I	5.77 ± 0.12	phase equil.	104
		7	phase equil.	62
		7.18	phase equil.	96
		6.00 ± 0.16	phase equil.	105
		6.3	phase equil.	93
		6.00 ± 0.01	direct (253 K, 3.4 MPa)	90
C_2H_6	I	7	phase equil.	62
		8.25	phase equil.	96
		8.24 ± 0.02	phase equil.	105
		7.67 ± 0.02	direct (253 K, 1.2 MPa)	90
C_3H_8		17	phase equil.	106
		17.95	phase equil.	96
		18	phase equil.	107
		19.7	phase equil.	108
		17.0 ± 0.1	direct (263 K, 0.3 MPa)	90
Ethylene oxide	I	6.89	density	69
Propylene oxide	II	17	Calvet calorimetry	74
		16.86	density	101
Tetrahydrofuran	II	17	Calvet calorimetry	78
		16.69	adiabatic calorimetry	27
2,5-Dihydrofuran	II	17	Calvet calorimetry	74
Cyclobutanone	II	17	dielectric study	80
1,3-Dioxolane	II	17	Calvet calorimetry	74
1,3-Dioxane	II	34	DTA	83
		17	Calvet calorimetry	74
Trimethylene	I	6.5	DTA	
oxide	II	17	DTA	84
				84
Acetone	II	17	DTA	85
1,4-Dioxane	II	36–39	DSC	86
Isoxazole	II	34	DTA	87
Isothiazole	II	34	DTA	88

The compositions of the str. I hydrates range between $M \cdot 5.75H_2O$ and $M \cdot 7.67H_2O$. This corresponds to full occupancy of the larger 14-hedral cages (3/4 of the total cage number) and incomplete occupancy of the smaller 12-hedral cage (1/4 of the total). For the light gases such as Xe and CH_4, about 70% of the 12-hedral cage is occupied, giving rise to the approximate formula $M \cdot 6H_2O$. For relatively larger guest molecules such as C_2H_6 and TMO, no 12-hedral cage is occupied, corresponding to $M \cdot 7.67H_2O$. On the other hand, most str. II hydrates have the composition of about $M \cdot 17H_2O$ corresponding to the full occupancy of the larger 16-hedral cages (1/3 of the total cage number). Only for the large guest molecules (650–700 pm), does occupancy of the 16-hedral cage become incomplete. The hydrates of 1,4-dioxane, isoxazole, and isothiazole have about a double hydration number ($M \cdot 34H_2O$).

It is remarkable that the occupancy at the decomposition pressure, corresponding to the possible minimum occupancy, is quite high for all the hydrates. This means that a large amount of guest molecule is required to stabilize the empty lattice which is less stable than ice. In the β-quinol clathrate [109], the occupancy of the guest can be changed down to the small occupancy region by controlling the guest-pressure at which the clathrate is formed. This enables one to determine the Langmuir constant at a given temperature and the thermodynamic properties of the empty lattice by the extrapolation method. Such analyses are not possible in clathrate hydrates.

5. Ideal solution model

The most important thermodynamic model to describe the non-stoichiometric nature of clathrate hydrates is the ideal solution model developed by van der Waals [110]. This model was first applied by him [111] to β-quinol clathrates which had only one kind of cage and was later extended to clathrate hydrates which had two kinds of cage. Details of the theory are described elsewhere [10, 13, 112] and so only the principle of the theory and the simple derivation of the important thermodynamic functions are described in section 5.1. As examples to which the theory was applied, two important thermodynamic studies are presented in section 5.2.

5.1. Derivation of the thermodynamic functions

The starting grand partition function is written in the form

$$Z = \exp(-F^\circ/kT) \sum_{N_{Mi}} \prod_i \left[\frac{N_i!}{(N_i - N_{Mi})! N_{Mi}!} (b_{Mi}\lambda_M)^{N_{Mi}} \right], \qquad (4)$$

where only a single guest molecule M is considered. F° is the free energy of water molecules in the empty lattice, N_1 and N_2 are the numbers of small and large cages respectively, and N_{M1} and N_{M2} the numbers of guest molecules in the respective cages. Two guest-dependent parameters λ_M and b_{Mi} are the absolute activity and the molecular partition function of M in cage i, respectively.

Equation (4) assumes that: (1), F° is independent of the degree of occupancy of the cages and nature of M, and (2), b_{Mi} is the same for each cage of the i-th type and independent of the occupancy of the cages. The first assumption is not strictly valid for large guest molecules which distort the lattice and the second is not strictly valid for guest molecules having strong polarity.

Applying the multinomial theorem to the summation in Eq. (4) we derive the following simple form

$$Z = \exp(-F^\circ/kT) \prod_i (1 + b_{Mi}\lambda_M)^{\nu_i N_W}, \tag{5}$$

where N_i has been replaced by $\nu_i N_W$. With an equilibrium distribution of M over the cages, all the familiar thermodynamic functions are related to Z by the equation

$$kTd(\ln Z) = (U/T)\,dT + pdV + N_M kTd(\ln \lambda_M) - \mu_W\,dN_W, \tag{6}$$

where N_M is the equilibrium number of encaged molecules of activity λ_M (i.e. $N_M = N_{M1} + N_{M2}$).

Occupancy of each cage θ_i can be shown to be of the form

$$\theta_i = b_{Mi}\lambda_M/(1 + b_{Mi}\lambda_M). \tag{7}$$

The activity of encaged molecules at fugacity f_M is

$$\lambda_M = f_M/(kT\phi_M), \tag{8}$$

where ϕ_M is the product of the translational, rotational, and internal partition functions of gaseous M. Equation (7) may be rewritten as the familiar Langmuir isotherm

$$\theta_i = C_{Mi}f_M/(1 + C_{Mi}f_M), \tag{9}$$

by substituting $C_{Mi}f_M$ for $b_{Mi}\lambda_M$. Here C_{Mi} is called the Langmuir constant which depends on T but only slightly on pressure.

The chemical potential is given from Eqs (6) and (9) by the form

$$\mu_W(H) = \mu_W^\circ + kT\sum_i \nu_i \ln(1 - \theta_i), \tag{10}$$

where μ_W° is the chemical potential of the empty lattice. Under the equilibrium conditions between the hydrate and ice (i.e. when $\mu_W(H) = \mu_W(I)$), the difference in

chemical potential between ice and the empty lattice is found to be

$$\Delta\mu_W(I \rightarrow H) = -kT\sum_i \nu_i \ln(1-\theta_i), \tag{11}$$

where the variation of $\Delta\mu_W(I \rightarrow H)$ with pressure is assumed to be zero at normal pressure. This equation determines the minimum cage occupancy and, through Eq. (9), the minimum pressure of M required for hydrate stability at a given temperature. Under the condition $\mu_W(H) < \mu_W(I)$, of course, various occupancies of the hydrate are possible.

From Eqs (5), (6), and (9), the internal energy is

$$U - U^\circ = N_W kT^2 \sum_i \nu_i \theta_i \partial(\ln b_{Mi})/\partial T, \tag{12}$$

where U° is the internal energy of the empty lattice. The change in enthalpy when one mole of M reacts with n moles of water can be derived from Eq. (12) to be

$$\Delta H(I + G \rightarrow H) = nN_A(U - U^\circ) - RT + n\Delta H(I \rightarrow E), \tag{13}$$

where N_A is the Avogadro number and $\Delta H(I \rightarrow E)$ the enthalpy difference between the empty lattice and ice.

To advance the calculation further, it is necessary to determine the form of the molecular partition function b_{Mi}. The model which is the simplest but which gives also excellent agreement with experimental is the spherical cell model originally used for liquid and compressed gas. Van der Waals and Platteeuw applied this model to clathrate hydrates by replacing the average radius of the cell formed by the neighbours in the liquid by the average radius a_i of the cage formed by z_i water molecules. The interaction energy between a guest and a water molecules is usually given by the Lennard–Jones 12–6 potential

$$4\varepsilon[(\sigma/r)^{12} - (\sigma/r)^6], \tag{14}$$

where ε is the energy depth at the separation of the van der Waals radius ($= 2^{1/6}\sigma$) and σ is the separation at which interaction energy becomes zero. In the present case, the values of ε and σ are given by the form

$$\varepsilon = (\varepsilon_W \varepsilon_M)^{1/2}, \qquad \sigma = (\sigma_W + \sigma_M)/2. \tag{15}$$

ε_M and σ_M can be evaluated from experimental data such as virial coefficient, viscosity, and molecular beam spectra, and from theory [113].

The molecular partition function b_{Mi} is given by

$$b_{Mi} = \phi_M\{\exp[-w_i(0)/kT]\}2\pi a_i^3 g_i, \tag{16}$$

where $w_i(0)$ is the energy at the cage center, and g_i the free volume integral. This function assumes that the rotational and vibrational contributions are the same as

in the free gas. This assumption is strictly valid for monoatomic guest molecules but not for polyatomic guest molecules. The functions $w_i(0)$ and g_i are expressed by the forms

$$w_i(0) = z_i\varepsilon(\alpha_i^{-4} - 2\alpha_i^{-2}), \quad \alpha_i = a_i^3/(\sigma^3 2^{1/2}) \tag{17}$$

$$g_i = \int \exp\{(z_i\varepsilon/kT)[-l(y)\alpha_i^{-4} + 2m(y)\alpha_i^{-2}]\} y^{1/2}\, dy \tag{18}$$

$$l(y) = (1 + 12y + 25.5y^2 + 12y^3 + y^4)(1-y)^{-10} - 1 \tag{19}$$

$$m(y) = (1+y)(1-y)^{-4} - 1 \tag{20}$$

$$y = r^2/a_i^2, \tag{21}$$

where r is the distance from the cage center. Thus all the thermodynamic functions can be calculated by using Eqs (9)–(13), (16)–(21) and appropriate values for ε and σ, if $\Delta\mu(\mathrm{I} \rightarrow \mathrm{E})$ and $\Delta H(\mathrm{I} \rightarrow \mathrm{E})$ are known.

The Kihara potential [114], which is adequate for polyatomic guest molecules is also used to express the guest-water interaction energy. Barrer and Edge [36] did not use the spherical cell model but summed the pairwise interactions between the guest molecules (Ar, Kr, Xe) and discrete water molecules in the unit cell. These advanced calculations are omitted here but described in detail elsewhere [10, 13, 112].

5.2. Thermodynamic analysis via the ideal solution model

The only one method to test the validity of the ideal solution theory without any knowledge on the molecular partition function b_{Mi} is to confirm the Langmuir isotherm by measuring the pressure dependence of occupancy of the hydrate at a constant temperature. As mentioned above, however, the occupancy of the hydrate cannot be changed much by changing the pressure at which the hydrate is formed. Barrer and Edge [36] have overcome this difficulty by an elegant method using the double hydrates. They observed the amount of Ar, Kr, and Xe absorbed into the $CHCl_3$ structure II hydrate at various constant pressures. Since all the large cages are occupied in advance by $CHCl_3$, rare gases effectively enter into only the smaller cages. Figure 5(a) shows the relation between the pressure and the volume of the Ar gas absorbed. The linearity of the plots clearly indicates the validity of the Langmuir isotherm. Figure 5(b) shows the plots of $\log K$ (K: Langmuir constant) *vs.* $1/T$ for Xe, Kr, and Ar gases. Each curve shows a good linearity and its slope gives the enthalpy of dissociation of each rare gas in the 12-hedral cage:

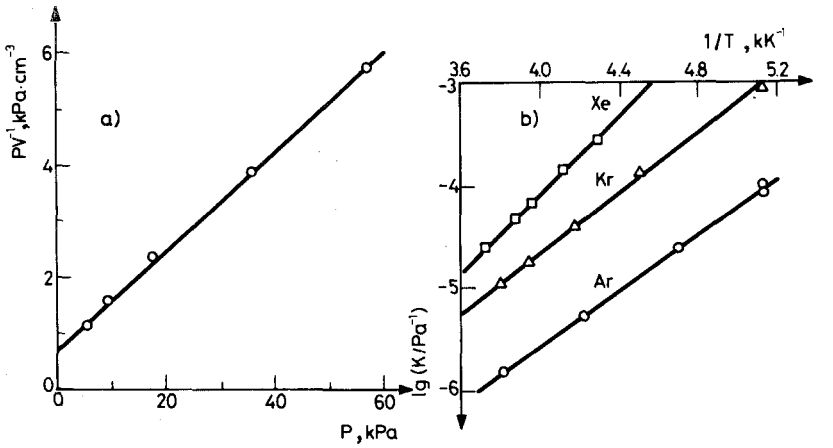

Fig. 5 (a) *p vs. P/v* plot of Ar hydrate (*P*: pressure of Ar gas, *v*: volume of Ar gas absorbed in the hydrate. (b) 10^3 K/*T vs.* $\log_{10} K$ plot of three rare gas hydrates (*T*: temperature, *K*: Langmuir constant) (Ref. [36])

Ar: 26 kJ mol^{-1}, Kr: 28 kJ mol^{-1}, Xe: 31 kJ mol^{-1}

These values agreed well with the theoretical values derived by Barrer and Edge [36] within the uncertainty of the estimation of the potential parameters.

To calculate the dissociation pressure p_M and the enthalpy of encagement ΔH(I + G → H) using the ideal solution model, the differences in chemical potential (for the former) and in enthalpy (for the latter) between ice and the empty lattice are required. In the past these values were frequently estimated by rough methods or neglected, but fairly good agreement between the theoretical and experimental values was obtained within the experimental errors and uncertainty of the parameters of the molecular partition function. Recently, as the experimental techniques were improved, several authors [115–119] tried to evaluate $\Delta\mu$(I → E) and ΔH(I → E). The most interesting and reliable work is by Handa and Tse [115]. They calculated $\Delta\mu$(I → E) and ΔH(I → E) based on the spherical cell model using the L–*y* potential and on their calorimetric [89, 102] and NMR [118] studies of Xe (str. I) and Kr (str. II) hydrates. The rare gases are the most suitable for the application of the ideal solution model and the spherical cell model. Before this study, however, Ar and Kr hydrates had not been analyzed in a reasonable way because before 1984 both hydrates had been believed to belong to the str. I [120]. The values obtained by Handa and Tse are as follows:

	$\Delta\mu(\mathrm{I} \rightarrow \mathrm{E})$,	$\Delta H(\mathrm{I} \rightarrow \mathrm{E})$,
	J mol^{-1}	J mol^{-1}
Structure I (Xe)	1287	931
Structure II (Kr)	1068	741

$\Delta\mu(\mathrm{I} \rightarrow \mathrm{E})$ of Xe was directly obtained by calorimetric ($n = 6.29 \pm 0.03$) [102] and ^{129}Xe–NMR study ($\theta_S/\theta_L = 0.73 \pm 0.02$) [118] by use of Eq. (11). Other values were evaluated from Eqs (7), (8), (11)–(13), (16)–(19) and the L–J parameters of guests (Xe: $\varepsilon_g/k = 225.3$ K, $\sigma_g = 406.9$ pm, Kr: $\varepsilon_g/k = 166.7$ K, $\sigma_g = 367.9$ pm) [112, 121] and water ($\varepsilon_w/k = 162$ K, $\sigma_w = 305$ pm), the latter set of which was determined so as to reproduce the calorimetric results on Xe ($n = 6.29$) and Kr ($n = 6.10$) [89]. This result clearly indicates that the empty lattice of the str. II is more stable than that of the str. I by 220 J mol^{-1} in chemical potential and by 177 J mol^{-1} in enthalpy. This is the reason why the smallest three guest molecules (Ar, Kr, O_2) hydrates take preferentially the str. II [25, 120]. The str. I hydrate is formed only when interaction between the guest and the 14-hedral cage (3/4 of the total) is sufficient to stabilize the structure. The guests Ar, Kr, O_2 are too small to provide this stabilization.

6. Heat capacity

The history of the heat capacity measurement of clathrate hydrates is fairly new compared with other thermodynamic properties described above. The first report of the heat capacity of clathrate hydrates is for THF and EO hydrates by Leaist et al. [71] in 1982 so that the previous reviews on clathrate hydrates have described nothing about the heat capacity.

The first column of Table 7 lists the clathrate hydrates whose heat capacities have been measured. The second column is the host structures, the third the temperature ranges studied, and the fourth the experimental methods. In earlier studies, attention was focused on the enthalpy of congruent melting or decomposition of the hydrates and so only the excess heat capacity was considered. Recently, however, some calorimetric studies were carried out on the heat capacity itself. They have given new insight into the problem of the molecular motions and the order-disorder phenomena of both guest and host molecules. In this chapter, some heat capacity data and their analyses are presented in three sections, each of which has a particular focus of interest.

Table 7 List of the clathrate hydrates whose heat capacities have been measured

Guest species	Str.	Temp. range, K	Method	Year	Ref.
Ar	II	12–130*	adiabatic	1988	28
Kr	II	85–270	Calvet	1986	89
		8–150	adiabatic	—	30
Xe	I	85–270	Calvet	1986	89
		8–170	adiabatic	—	30
CH_4	I	85–270	Calvet	1986	90
C_2H_6	I	85–270	Calvet	1986	90
C_3H_8	II	85–270	Calvet	1986	90
Cyclopropane	I	240–260	DSC	1983	34
	II	240–260	DSC	1983	34
Ethylene oxide	I	120–260	Calvet	1982	71
		245–270	DSC	1983	34
		6–300	adiabatic	1988	29
Propylene oxide	II	95–260	Calvet	1985	74
Tetrahydrofuran	II	120–260	Calvet	1982	71
		245–270	DSC	1983	34
		85–270	Calvet	1984	78
		17–261	adiabatic	1985	122
		6–300*	adiabatic	1988	27
2,5-Dihydrofuran	II	95–260	Calvet	1985	74
1,3-Dioxolane	II	95–260	Calvet	1985	74
1,3-Dioxane	II	95–260	Calvet	1985	74
Trimethylene oxide	Mix.+	85–230	adiabatic	1983	123
	Mix.+	85–230	Calvet	1985	124
	II	85–230	Calvet	1985	124

* KOH-doped sample has also been measured.

+ Mixture of str. I and II.

6.1. Additivity of the heat capacities of the guest and host

A common interest in clathrate compounds is the additivity of heat capacities of the guest and host, and the model which reproduces the heat capacities of both components. Extensive studies were done on β-quinol clathrate compounds [109]. The situation becomes complicated by virtue of the two kinds of cavity in the case of clathrate hydrates. These problems were first investigated roughly in the earlier heat capacity studies of the cyclic ether hydrates [74, 78]. However, the most suitable system to investigate these problems must be the hydrates of the rare gases which have no intramolecular and rotational degrees of freedom, and which interact with the host water molecules via the simple van der Waals interaction. In the Ar- and Kr-β-quinol clathrates whose cage diameters are almost the same as that of 12-hedral cage of the clathrate hydrate (780 pm), heat capacity at a given temperature

was a linear function of the occupancy, implying that the additivity of the heat capacities of the guest and host is a valid assumption.

The heat capacity measurement of the rare gas hydrates is quite difficult because they are stable only at high pressure and low temperature conditions, and it takes a long time to complete the formation. Furthermore, the extent of the formation (if the formation is not complete) and the composition must be determined to obtain the quantitative heat capacity value. Handa [89] first measured the heat capacities of Xe and Kr hydrates in the temperature range above 85 K with the heat flow calorimeter described above. Heat capacity study from low temperature was recently performed by our group [28, 30] for the three rare gas hydrates with an adiabatic calorimeter.

Figure 6 shows schematically the adiabatic calorimeter [125] used in our study. This calorimeter was constructed originally in order to measure the heat capacity of a solid sample at constant high-pressure up to 250 MPa. Most of the cryostat is the same as an ordinary adiabatic calorimeter except for the pressure transmitting tubes

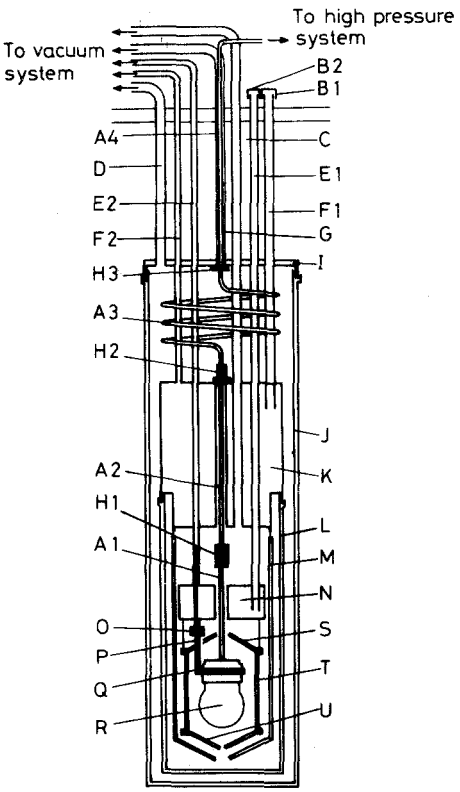

Fig. 6 Schematic drawing of an adiabatic calorimeter used for the rare gas hydrates (Ref. [125])

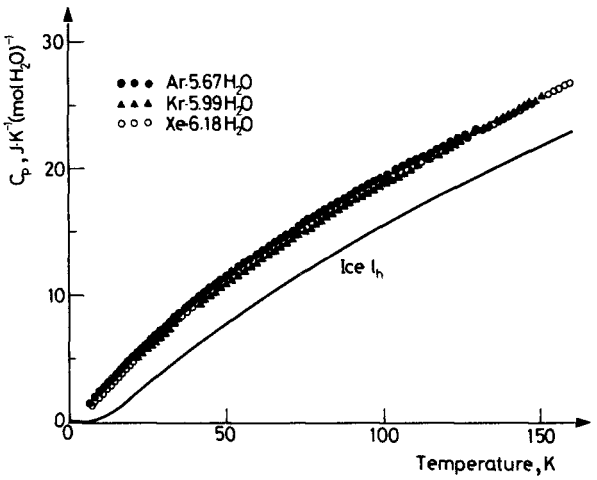

Fig. 7 Heat capacities of the three rare gas hydrates (Ref. [28, 30])

(A1–A4) through which the pressure medium (usually helium gas) flows into and out, and which is connected to the calorimetric cell. Temperatures of all the tubes are controlled so as to keep the adiabatic condition during the heat capacity measurement.

The hydrate samples were synthesized in situ from water and the respective high-pressure (Ar: 200 MPa, Kr: 8.3 MPa, Xe: 3.0 MPa) gases inside the cell. The pressure was kept almost constant by supplying the gas from the external high-pressure system through the high-pressure tubes. The formation was found to be accelerated by temperature cycles across the melting point of ice. Even with this acceleration effect, it took 2–3 weeks to obtain an almost-complete hydrate sample. The extent of the formation was determined by measuring the enthalpy of melting of the remaining ice. Heat capacity measurements of Xe and Kr hydrates were carried out at around the dissociation pressure of the respective hydrates. The compositions of the three hydrates were determined to be $Kr\cdot 5.99H_2O$ and $Xe\cdot 6.18H_2O$ by evaluating the amount of the guest gas released at the dissociation and to be $Ar\cdot 5.67H_2O$ (maximum hydration number) by calculation using the ideal solution theory and an extrapolated value of the Langmuir constant due to Barrer and Edge [36].

Figure 7 shows the heat capacities of the three hydrates represented per mole of H_2O. No anomaly due to any phase or glass transition was observed. The line in the figure represents the heat capacity of hexagonal ice [126]. There is, of course, no criterion as to how to divide the experimental heat capacity into the contributions from the host and guest. Hence, as the first approximation, we assumed that the simple additivity of the heat capacities of the guest and host is valid, and the heat

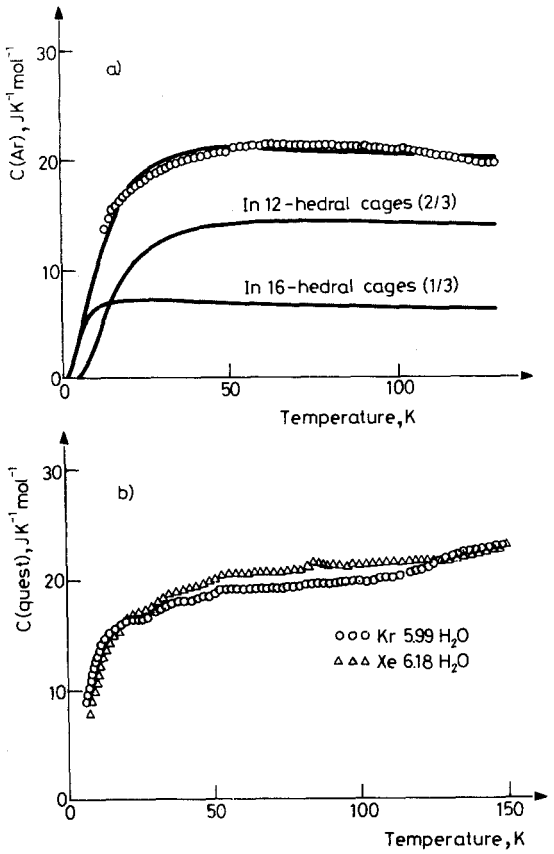

Fig. 8 Molar heat capacities of the encaged guest molecules. (a) Ar, (b) Kr and Xe (Ref. [28, 30])

capacity of the host is the same as that of hexagonal ice. The heat capacities of the guests calculated in this way are shown in Fig. 8(a) for Ar and 8(b) for Kr and Xe, both represented per mole of the guest.

In the discussion so far, the classical statistical model has been used to describe the guest motions in the cage because the temperature considered was high enough. To discuss the low-temperature heat capacity of the guest, however, the quantum statistical partition function is required. The motion of the guest atom in the cage is called rattling, which is the motion in limited space and is intermediate in nature between harmonic oscillation and free translation. By assuming spherical cage symmetry, the potential function relevant to this motion is reasonably described by the one-dimensional Pöschl–Teller potential [127, 128],

$$V(x) = \frac{h^2 a(a-1)}{8md_0^2 \sin^2[(x/d_0)+1/2]}, \tag{22}$$

where h is Planck's constant, m the mass of the guest molecule, d_0 the distance through which the guest molecule can move in the cage, and a is a parameter reflecting the stiffness of the cage wall—the larger a the stiffer the cage wall. The energy levels of the potential are given by the simple analytical form

$$E_n = (h^2/8md_0^2)(a+n)^2 \qquad n = 0, 1, 2, \ldots, \tag{23}$$

where n is the quantum number.

Since both hydrate structures (I and II) have two types of cage, five unknown parameters remain to be determined: i.e. a(L), a(S), d_0(L), d_0(S), and θ_S/θ_L. In the Ar hydrate, the two parameters a(S) and d_0(S) were determined so as to reproduce the experimental heat capacities by the least squares fitting assuming a(L) = a(S), d_0(L) − d_0(S) = 160 pm (the geometrical difference in cage diameter), and $\theta_S/\theta_L = 1$. There was a good fit as shown in the figure. The contribution from each cage is calculated separately as also shown in the figure. The parameters determined were as follows: a(S) = 18.5, d_0(S) = 215 pm. These are both reasonable in magnitude compared with the values of the Ar-β-quinol clathrate (a = 23, d_0 = 240 pm), which are obtained from a far-infrared study [128]. This successful result of the fitting gives indirect evidence for the validity of the underlying assumptions in the Ar hydrate.

We also tried a similar analysis for the Kr and Xe hydrates. However, the heat capacities of both guests could not be reproduced even though all the five parameters were treated as adjustable. These failures of the fitting are clearly due to the experimental heat capacities in the high temperature region, which increase with temperature. The heat capacity function derived by the Pöschl–Teller potential can not reproduce such a heat capacity curve; i.e., the heat capacity decreases with temperature in the high temperature region. For the Xe hydrate, the heat capacity could be reproduced only in the low temperature region (< 70 K). These results indicate that at least one of the employed assumptions used is not valid for the Xe and Kr hydrates. This seems to be related to the larger guest-host interactions of the Kr and Xe hydrates, which result in larger coupling between the lattice vibration of the host and the rattling motion of the guest, and/or the anharmonicity of the host lattice vibration. In the hydrates of more bulky EO and THF, large thermal expansivity due to the anharmonicity of the lattice has actually been observed in an X-ray diffraction study [129] and reasonably explained by the guest-host interaction in a molecular dynamics calculation [130].

6.2. Order-disorder in the water reorientation

Water molecules in clathrate hydrates are disordered in their orientations. In general, such disorder disappears through a phase transition on cooling.

Nevertheless, previous dielectric and NMR studies have not shown any phase transition down to temperatures as low as 4 K. This situation is the same as for ice Ih and Ic. In these ices, however, glass transitions have been observed in calorimetric studies [126, 131] and it has been confirmed that the water reorientation becomes frozen-in in its short-range ordered state before the hypothetical ordering transition takes place at a lower temperature. In clathrate hydrates, it is important to confirm the existence or otherwise of the glass transition and, if it exists, to clarify its nature for various guest species. Calorimetric studies are quite suitable for this purpose because the relaxation time of the water reorientation around the possible glass transition is long ($\sim 10^6$ s) compared with the time scale of dielectric or NMR studies.

The clathrate hydrates measured by us are those of the following five guest species:

guest	Ar [28]	Kr [30]	Xe [30]	EO [29]	THF [27]
structure	II	II	I	I	II
polarity	n	n	n	p	p
	(non-polar)			(polar)	

These guest molecules were chosen in order to investigate the effects of both the host structure and the polarity of the guest on the water reorientation. The hydrate crystals of EO and THF were easily obtained by allowing the stoichiometric

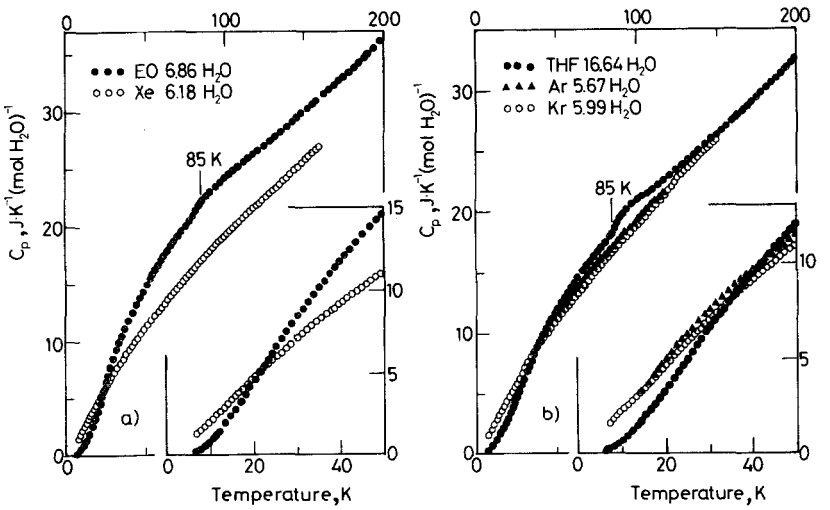

Fig. 9 Heat capacities of (a) the str. I (EO and Xe) and (b) the str. II (Ar, Kr, and THF) clathrate hydrates (Ref. [27–30])

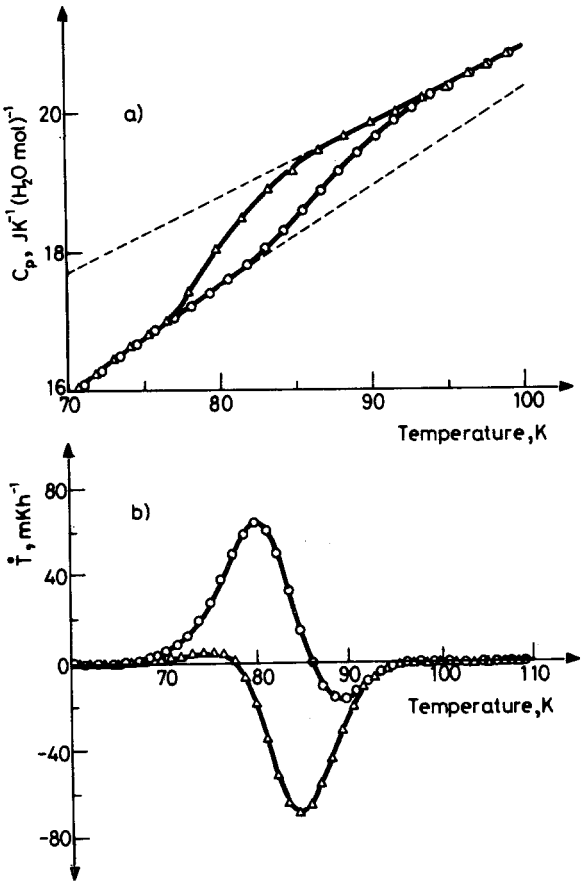

Fig. 10 (a) Heat capacities and (b) corresponding temperature drift rates of THF hydrate. ○: cooled at 2.7 deg min^{-1}, △: annealed at 78 K for 44 h

solution to solidify in an ordinary adiabatic calorimeter cell [27]. The formation of the rare gas hydrates has already been described in the last section.

Figures 9(a) and 9(b) show the heat capacities of the hydrates which belong to the str. I and II, respectively. In all the hydrates, no phase transition was observed. However, a definite but small jump of heat capacity was found around 85 K for the EO a ıd THF hydrates. Heat capacity around the anomaly in the THF hydrate is shown in Fig. 10(a) on an enlarged scale and the corresponding spontaneous temperature drift rate observed in each equilibration period of the heat capacity measurement is in Fig. 10(b). In the sample cooled at the rate of 2.7 K min^{-1} (○), an exothermic followed by an endothermic drift appeared in the temperature range 65–95 K. On the other hand, in the sample annealed at 78 K for 44 h (△), only an

endothermic drift appeared starting from the annealing temperature. The corresponding heat capacity curves exhibit a jump around the temperature at which the drift changes from positive to negative. For the EO hydrate, substantially the same phenomena were observed. Both the temperature drifts and the corresponding heat capacity jump are typical behaviour in the glass transition region [132, 133]. Taking into account the fact that the relaxation time of the water reorientation is expected to become 10^3 s around 90 K from the dielectric studies of both hydrates [79, 134], these glass transitions are considered to arise from the freezing of the water reorientational motion.

The excess heat capacities above the glass transitions of the EO and THF hydrates are shown in Fig. 11. These were derived by subtracting the normal heat

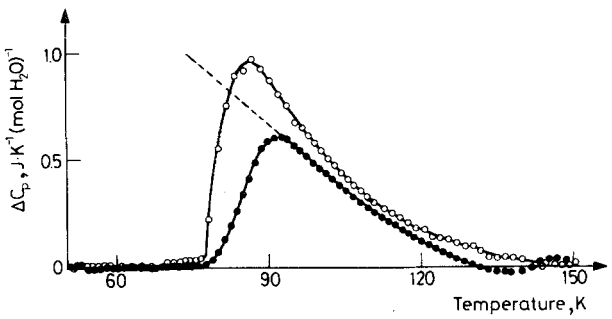

Fig. 11 Excess heat capacities of $EO \cdot 6.86H_2O$ (●) and $THF \cdot 16.64H_2O$ (○) in the temperature range of the glass transition

capacities (base lines) determined by joining smoothly the data below 80 K and above 140 K, both of which are considered to be free from the anomaly. The excess heat capacities increase with decreasing temperature and suddenly diminish at the glass transitions. These are quite similar to the glass transitions of ice II_h [126] and Ic [131] and indicate that short-range ordering of the proton configurational mode occurs progressively with decreasing temperature and becomes frozen in at the glass transition. Water reorientation in the rare gas hydrates is also expected to be frozen in around 100 K from dielectric studies [135, 136]. Hence, the absence of glass transition in the calorimetric study indicates that short-range order does not develop significantly around 100 K in the rare gas hydrates.

Adiabatic calorimetry is quite effective not only to obtain the absolute values of heat capacity but also to investigate spontaneous processes whose relaxation time is as long as 10^6 s [137]. The relaxation time τ of the motion related to the glass transition (the water reorientation in this case) can be calculated at a given

temperature T by assuming the equation

$$\tau(T) = [H(T, t) - H(T, \infty)]/[\mathrm{d}H(T, t)/\mathrm{d}t]. \quad (24)$$

The numerator of the equation is the difference between the enthalpies at time t and at the respective equilibrium state. These quantities can be obtained from the total enthalpy actually relaxed before reaching the equilibrium state and the integration of the excess heat capacity, respectively. The denominator is the enthalpy relaxation rate and is obtained from the temperature drift rate multiplied by the heat capacity of the calorimetric cell. Figure 12 shows the relaxation times thus obtained in the exothermic drift region of the glass transitions of the EO and THF hydrates. Both curves seem to be linear at lower temperature but, especially for EO hydrate, deviating from linearity at higher temperatures. These observations are considered to be related to a distribution of relaxation times but any quantitative analysis for the distribution has not yet been performed. The effective activation enthalpies in the lower temperature region are calculated from the Arrhenius equation

$$\tau(T) = \tau_0 \exp(\Delta H^{\neq}/RT). \quad (25)$$

The values for both hydrates, corresponding to the slopes of the straight lines, are shown in the figure. These are almost the same as each other and close to that of ice Ih (18–20 kJ mol^{-1}) [126]. This indicates that water reorientation in both host

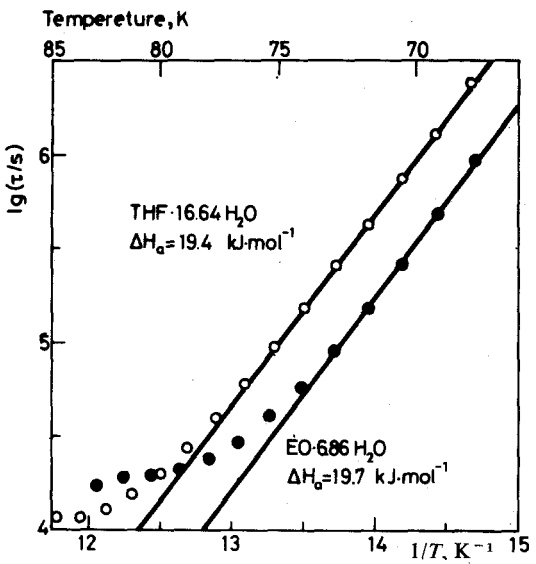

Fig. 12 Arrhenius plots of the relaxation times of EO · 6.86H_2O (●) and THF · 16.64H_2O (○) (Ref. [27, 29])

structures in the glass transition region follows as the process of migration of the Bjerrum defects [138] produced by external impurities, as in the case of ice Ih.

Thus, the relaxation time, the effective activation enthalpy, and the excess heat capacity of the water reorientational mode are little affected by the difference of the host structure. However, the water reorientational mode is strongly affected by the polarity of the guest molecules in the sense that the glass transition is observed only for the polar guest hydrates (EO and THF) but not for the non-polar ones (Ar, Kr, Xe).

In ices, it is well-known that the water reorientational motion is accelerated by doping the samples with trace amounts of impurity. The most effective dopants tested so far are alkali hydroxides. Tajima et al. first found a first-order transition at 72 K in KOH (ca. 10^{-4} mole fraction)-doped ice Ih by a calorimetric study [139]. The independence of the transition temperature from the kind of alkali hydroxide and concentration of the dopant [140] indicate that the transition is an intrinsic property of pure ice Ih. The low-temperature phase ($Cmc2_1$) has been confirmed to be a proton ordered state by neutron diffraction study [141] and was designated as ice XI [142]. The acceleration mechanism of the water reorientation is still not clear but is believed to be related to ionic L defects (defects combining ionic and orientational faults) produced by the doping. We applied this method to the str. II Ar [28] and THF [26, 27] hydrates. The mole fractions of the dopant (KOH) to water were 1.3×10^{-3} and 1.8×10^{-4}, respectively.

In the Ar hydrate, a glass transition related to the freezing of the water reorientational motion was found at 55 K. This indicates that the freezing temperature of the water reorientation was lowered down to the temperature where the short-range order developed even slightly.

In the THF hydrate, a more drastic change was induced by the doping. Figure 13 shows the heat capacity of the pure and KOH-doped THF hydrates. Both of the heat capacity curves are almost the same above T_g. In the temperature range below T_g, however, the doped sample did not undergo a glass transition but a first-order transition at 62 K. The transition temperature was independent of the mole fraction of the dopant [143] as in the case of ice Ih. This transition was observed also in a recent dielectric study [144]. Figure 14 shows the dielectric constant ε' (upper) and the loss ε'' (lower) of the THF hydrates. Open and closed symbols stand for data for the pure and doped samples, respectively. In the doped sample, the dispersion region of the water reorientation is clearly shifted down to lower temperatures. The real part ε' suddenly decreases and the loss component ε'' disappears almost completely at the transition (62 K). These facts indicate that the water reorientation is accelerated sufficiently by the doping and the water dipoles become ordered completely without leaving any disorder within the time scale of the dielectric experiment.

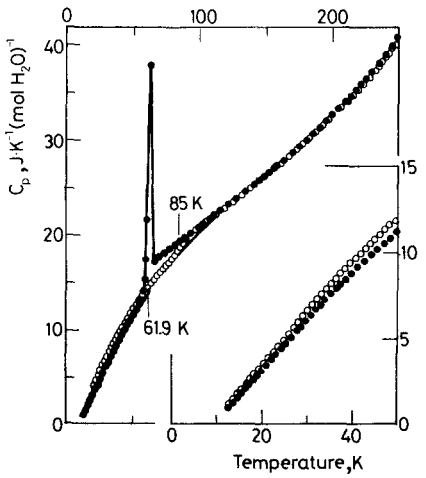

Fig. 13 Heat capacities of pure (○) and KOH ($x = 1.8 \times 10^{-4}$)-doped (●) THF hydrates (Ref. [26, 27])

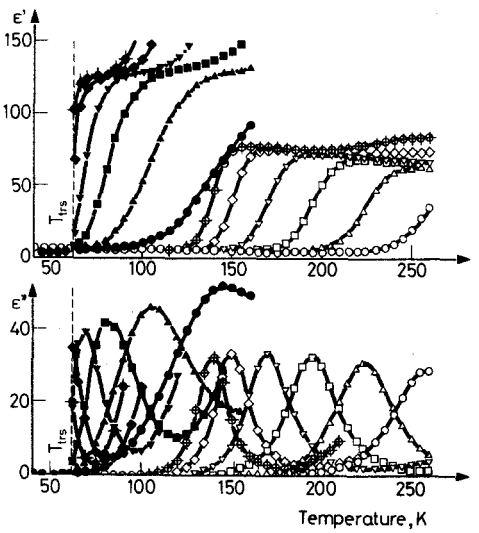

Fig. 14 Temperature dependence of ε′ (upper) and ε″ (lower) of the pure (open symbols) and KOH ($x = 1.8 \times 10^{-4}$)-doped (closed symbols) THF hydrates. ○: 1 MHz, △: 100 kHz, □: 10 kHz, ▽: 1 kHz, ◇: 100 Hz, ⊕: 20 Hz (Ref. [144])

Figure 15 shows the excess heat capacities due to the transitions of the KOH-doped THF hydrate and KOH (1.8×10^{-3} mole fraction)-doped ice Ih [140]. The transition temperature of the THF hydrate is 10 K lower than that of ice Ih, and the high-temperature-side tail of the transition of the THF hydrate, corresponding to the magnitude of the short-range ordering, is larger than that of ice Ih. On the whole, however, both the curves are closely similar.

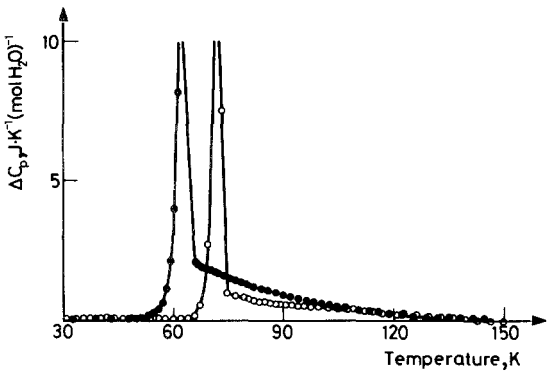

Fig. 15 Excess heat capacities due to the transition of KOH ($x = 1.8 \times 10^{-4}$)-doped THF hydrate (●) and KOH ($x = 1.8 \times 10^{-3}$)-doped hexagonal ice (○) (Ref. [28])

The transition entropy of the THF hydrate is 2.36 J K^{-1} (H_2O mol)$^{-1}$. However, all this quantity is not due to the ordering of the water reorientation because the heat capacity of the doped sample is considerably smaller than that of the pure one below the transition. In the temperature range below 85 K (the glass transition temperature), the water reorientation of the pure sample is frozen-in and therefore the difference between both heat capacities should be ascribed to some mode other than the water reorientation. By integrating the heat capacity difference from 0 to 62 K, the entropy due to the mode is calculated to be 0.83 J K^{-1} (H_2O-mol)$^{-1}$. The entropy due to the water ordering becomes the remaining 1.53 J K^{-1} (H_2O-mol)$^{-1}$, which is smaller than the expected values: i.e., 67% of that of the KOH-doped ice Ih (2.3 J K^{-1} mol^{-1} [140]) and 45% of the theoretical value (3.37 J K^{-1} mol^{-1} [145]) for the four-coordinated hydrogen-bond network satisfying the ice conditions [21]. Two reasons seem to be possible to explain the experimental entropy. One is that the high temperature phase is partially ordered and the effect of the ordering is buried in the so-called "normal" heat capacity so as to reduce the apparent entropy of the transition. The other is that the low temperature phase is partially ordered and the remaining disorder is frozen-in simultaneously with the transition. The first possibility can be examined by the measurement of the absolute entropies of both pure and KOH-doped THF hydrates. The precise heat capacity and $p-T-x$ phase diagram of the gas-liquid equilibrium of the THF-water system are required for this. The second possibility will be examined by a structural study of the low temperature phase.

6.3. Order-disorder in the guest reorientation

The only hydrate which exhibits an ordering transition of the guest orientation is str. I trimethylene oxide (TMO) hydrate. The reason why no guest ordering

transition has been observed in other hydrates is explained as follows: The guest-guest interaction energy is so small, especially in str. II hydrate, that the fluctuating electric field induced by the orientationally disordered water molecules overrides it. Because the symmetry of the hydrate cage, except the 14-hedral one, is quite high, guest molecules have a great deal of orientational freedom. The TMO molecules are enclathrated only in the 14-hedral cage which is arranged like a column in the lattice and the TMO dipole moment is fairly large (1.9 Debye).

The ordering transition of TMO hydrate was first found in dielectric and NMR studies by Gough et al. [146]. Figure 16 shows the dielectric constant ε' and the corresponding loss ε'' of the TMO hydrate. The static dielectric constant due to the guest rotational motion ($\varepsilon_{02} = \varepsilon_{\infty 1}$), which is represented by the higher heavy line, decreases steeply at the temperature around 105 K. Below 105 K, however, ε' again becomes dependent on frequency, implying that TMO molecules are still orientationally disordered to some extent. A discontinuity was observed also in the temperature dependence of second moment in the proton NMR study. From these experimental results and the calculation on the guest-guest and guest-host interaction energies, Gough et al. suggested that most TMO molecules undergo a phase transition at 105 K below which TMO dipoles are parallel to the $\bar{4}$ axis of the 14-hedral cages.

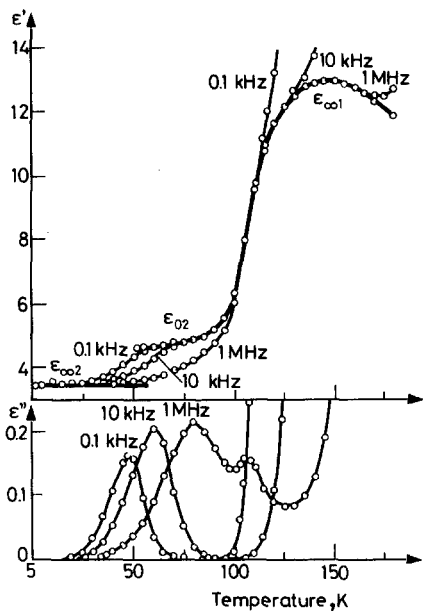

Fig. 16 Temperature dependence of ε' (upper) and ε'' (lower) of str. I TMO hydrate (Ref. [146]). The upper and lower heavy lines represent ε_{02} ($= \varepsilon_{\infty 1}$) and $\varepsilon_{\infty 2}$, respectively

Recently, Handa [124] performed a calorimetric study of both str. I and II. TMO hydrates with the heat flow calorimeter already mentioned. Figure 17 shows the heat capacity curves of $TMO \cdot 7.30H_2O$ (curve 1), $TMO \cdot 7.65H_2O$ (curve 2), $TMO \cdot 8.06H_2O$ (curve 3), and $TMO \cdot 17H_2O$ (curve 4). The stoichiometric compositions of the str. I. and str. II TMO hydrates are $TMO \cdot 7.67H_2O$ and

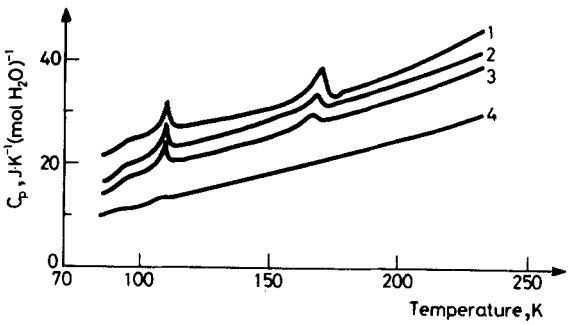

Fig. 17 Heat capacities of TMO hydrates. Curve 1: $TMO \cdot 7.30H_2O$, curve 2: $TMO \cdot 7.65H_2O$, curve 3: $TMO \cdot 8.06H_2O$, curve 4: $TMO \cdot 17H_2O$. Curves 2, 3 and 4 have been shifted downward by 6, 8 and 8 $J\ K^{-1}\ (H_2O\text{-mol})^{-1}$ (Ref. [124])

$TMO \cdot 17H_2O$, respectively. All the samples were prepared by keeping them 1–15 K below their dissociation temperatures for about 60 days. There are two distinct thermal anomalies, one lying around 107 K and the other around 168 K. The latter peak was ascribed to the eutectic melting of TMO and the str. I (and possibly TMO and the str. II). The appearance of this peak indicates that the $TMO \cdot 17H_2O$ sample has almost homogeneous str. II but the other samples are the mixtures of str. I, str. II and TMO. The peak around 107 K is due to the transition of the guest orientational ordering because the peak appears only in the str. I and its temperature is quite close to that of the transition observed in the dielectric and NMR studies [146]. The entropy of transition is 1.3 $J\ K^{-1}$ $(TMO\text{-mol})^{-1}$, corresponding to R ln 1.2. This value seems to be quite small if the TMO molecules are completely ordered at the transition because they have a great deal of orientational freedom, at least more than R ln 2 in entropy, in the high temperature phase. This result is consistent with the dielectric and NMR results that TMO molecules are still orientationally disordered in the low temperature phase.

Figure 18 shows the dielectric data of the THF hydrates corresponding to the low temperature part of Fig. 16. In the pure sample, the dielectric dispersion due to the guest reorientation is observed in the temperature range below 50 K. In the KOH-doped sample, however, ε' falls at the transition to the value corresponding to the high frequency limit and any appreciable dispersion is no longer observed. These

results suggest that the THF molecules are also orientationally ordered simultaneously wih the orientational ordering of the water molecules.

In the str. II THF hydrate, the THF molecules are enclathrated only in the 16-hedral cages which are almost spherical, at least having tetrahedral symmetry, in the water disordered state. Taking into account the fact that the guest-host electrostatic interaction is much larger than the guest-guest one [147], the ordering of THF molecules, if any, should be attainable by the occurrence of some non-tetrahedral electrostatic field in the 16-hedral cages produced by the water orientational ordering.

The difference in heat capacity between the pure and doped samples is considered to be due to the change of rotational motion of the THF molecules associated with the water ordering. If the THF dipole preferably orients one of four hexagons of the 16-hedral cage as in the case of TMO molecule in the 14-hedral cage, the configurational entropy should become $R \ln 4$ ($= 11.5$ J K^{-1} (THF-mol)$^{-1}$). The experimental entropy derived by integrating the heat capacity difference (0.83 J K^{-1} (H_2O-mol)$^{-1}$ = 13.6 J K^{-1} (THF-mol)$^{-1}$) is similar to this value.

In the last section, it was shown that the appearance of the glass transition depends on the guest molecules. In this section, it was shown that the orientational freedom of the guest molecules is strongly affected by the ordering of the host water reorientation. Thus, the coupling between the host and the guest exists both in the short- and long-range ordered states of the water reorientation. At the present stage, the polarity of the guest molecule seems to be the most important factor in

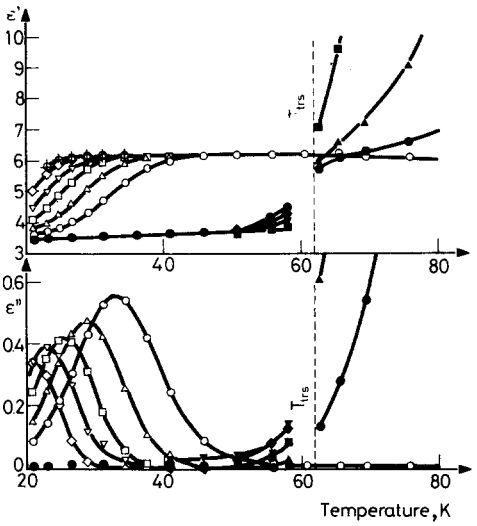

Fig. 18 The low-temperature part of dielectric constant and loss of THF hydrate (Ref. [144])

determining the magnitude of the coupling. To investigate further the mechanism of the coupling, precise calorimetric studies of the doped and pure hydrates of different kinds of guest molecule should be performed. TMO hydrate is especially interesting because it is the only system in which one can investigate the water reorientational motion in the guest-ordered state.

* * *

We would like to thank Associate Professor Masaharu Oguni in Tokyo Institute of Technology and Dr. Paul Handa in National Research Council of Canada for their useful discussions. We also wish to thank Professor R. G. Ross in University of Umeå for his critical reading and grammatical improvement of the manuscript. Thanks are extended to Miss Noriko Onoda for her assistance in making figures used in this review. Parts of the works described here were supported by the Nissan Science Foundation, to whom the authors' thanks are due.

References

1 "Inclusion Compounds", eds J. L. Atwood, J. E. D. Davies and D. D. MacNicol, Academic Press, London 1984.
2 H. Davy, Phil. Trans. Roy. Soc. (London), 101 (1811) 1.
3 M. von Stackelberg, Naturwiss., 36 (1949) 327, 359.
4 M. von Stackelberg and H. R. Müller, Z. Electrochem., 58 (1954) 25.
5 K. A. Kavenvolden and M. A. McMenamin, U.S. Geol. Surv. Cire., (1980) 825.
6 "Handbook of Gas Hydrate Properties and Occurrence", U.S. Department of Energy Publication DOE/MC/19239–1546, December (1983).
7 I. Ridley and K. Dominic, New Scientist, 25 February (1988).
8 G. A. Jeffrey, in "Inclusion Compounds", eds J. L. Atwood, J. E. D. Davies and D. D. MacNicol. Academic Press, London 1984, Vol. 1, Chap. 5.
9 D. W. Davidson and J. A. Ripmeester, in "Inclusion Compounds", eds J. L. Atwood, J. E. D. Davies and D. D. MacNicol, Academic Press, London 1984, Vol. 3, Chap. 3.
10 B. Berecz and M. Balla-Achs, "Gas Hydrates", Studies in Inorganic Chemistry 4, Elsevier, Amsterdam 1983.
11 Y. F. Makogon, "Hydrates of Natural Gas", translated by W. J. Cieslewicz, PennWell, Tulsa 1981.
12 C. I. Ratcliffe and J. A. Ripmeester, Newsleter of "order/disorder in solids", ed. R. Weir 6, No. 4, (1988) 33.
13 D. W. Davidson, in "Water: A Comprehensive Treatise" (ed. F. Franks), Plenum Press, New York 1973, Vol. 2, Chap. 3.
14 J. A. Ripmeester, T. S. Tse, C. I. Ratcliffe and B. M. Powell, Nature, 325 (1987) 135.
15 D. W. Davidson, S. R. Gough, Y. P. Handa, C. I. Ratcliffe, J. A. Ripmeester and J. S. Tse, J. Phys. (Paris), Colloq. C1, 3 (1987) 537.
16 K. W. Allen and G. A. Jeffrey, J. Chem. Phys., 38 (1963) 2304.
17 S. L. Miller, S. R. Gough and D. W. Davidson, J. Phys. Chem., 81 (1977) 2154.
18 R. K. MacMillan, G. A. Jeffrey and T. H. Jordan, J. Chem. Phys., 47 (1967) 1229.
19 D. Londono, W. F. Kuhs and J. L. Finney, Nature, 332 (1988) 141.
20 N. H. Fletcher, "The Chemical Physics of Ice", Cambridge Univ. Press (1970).
21 J. D. Bernal and R. H. Fowler, J. Chem. Phys., 1 (1933) 525.
22 R. K. McMullan and G. A. Jeffrey, J. Chem. Phys., 42 (1965) 2725.

23 T. C. W. Mak and R. K. McMullan, J. Chem. Phys., 42 (1965) 2732.
24 F. Hollander and G. A. Jeffrey, J. Chem. Phys., 66 (1977) 4699.
25 J. S. Tse, Y. P. Handa, C. I. Ratcliffe and B. M. Powell, J. Incl. Phenom., 4 (1986) 235.
26 O. Yamamuro, M. Oguni, T. Matsuo and H. Suga, Solid State Commun., 62 (1987) 289.
27 O. Yamamuro, M. Oguni, T. Matsuo and H. Suga, J. Phys. Chem. Solids, 49 (1988) 425.
28 O. Yamamuro, M. Oguni, T. Matsuo and H. Suga, J. Incl. Phenom., 6 (1988) 307.
29 O. Yamamuro, Y. P. Handa, M. Oguni and H. Suga, J. Incl. Phenom., submitted for publication.
30 Y. P. Handa, O. Yamamuro, M. Oguni and H. Suga, J. Chem. Thermodyn., in press.
31 L. D. Sortland and D. B. Robinson, Can J. Chem. Eng., 42 (1964) 38.
32 D. R. Hafemann and S. L. Miller, J. Phys. Chem., 73 (1969) 1392.
33 Y. A. Majid, S. K. Garg and D. W. Davidson, Can. J. Chem., 47 (1969) 4697.
34 J. E. Callanan and E. D. Sloan, Int. Gas Res. Conf., (1983) 1012.
35 J.-C. Rosso and L. Carbonnel, Compt. Rend. Acad. Sci. Paris, 274C (1972) 1108.
36 R. M. Barrer and A. V. J. Edge, Proc. Roy. Soc., Ser., A 300 (1967) 1.
37 D. R. Marshall, S. Saito and R. Kobayashi, AIChE J., 10 (1964) 202, 723.
38 R. de Forcrand, Compt. Rend., 176 (1923) 355.
39 R. de Forcrand, Compt. Rend., 181 (1925) 15.
40 A. van Cleeff and G. A. M. Diepen, Rec. Trav. Chim. Pays-Bas, 84 (1965) 1085.
41 W. M. Deaton and E. M. Frost, Gas, 16 (1940) 28.
42 W. M. Deaton and E. M. Frost, Proc. Nat. Gas Dept., AGA, (1940) 122.
43 E. M. Frost and W. M. Deaton, Proc. Nat. Gas. Dept., AGA, (1946) 49.
44 R. Kobayashi and D. L. Katz, Petr. Tr. AIME, 186 (1949) 66.
45 H. H. Reamer, F. T. Selleck and B. H. Sage, Petr. Tr. AIME, 195 (1952) 197.
46 S. L. Miller, Proc. Nat. Acad. Sci. U.S., 47 (1961) 1798.
47 A. van Cleeff and G. A. M. Diepen, Rec. Trav. Chim., 81 (1962) 426.
48 D. A. Wilms and A. A. van Haute, in "Proc. Third Int. Symp. Fresh Water from the Sea", eds A. Delyannis and E. Delyannis, Athens 1970, Vol. 3, p. 117.
49 S. Sh. Byk and V. I. Fomina, Doklady A. N. SSSR, 204 (1972) 123.
50 J. Kass, Dissert., Syracuse Univ. 1967.
51 D. B. Robinson and B. R. Mehta, J. Can. Petr. Techn., 1 (1971) 32.
52 S. D. Larsen, Dessert, Univ. of Illinois 1955.
53 P. Villard, Ann. Chim. Phys. Ser., 7, 11 (1897) 289.
54 F. T. Selleck, L. T. Carmichael and B. H. Sage, Ind. Eng. Chem., 44 (1952) 2219.
55 F. E. C. Scheffer, Proc. Kon. Nerderl. Akad. Wetensch., 13 (1911) 829.
56 A. E. Korvezee, F. E. C. Scheffer, Rec. Trav. Chim. Pays-Bas., 50 (1931) 256.
57 R. M. Wright and O. Mass, Can. J. Research, 6 (1932) 94.
58 J. G. Van Berkum and G. A. M. Diepen, J. Chem. Thermodyn., 11 (1979) 317.
59 G. Tammann and G. Kriege, Z. Anorg. Allg. Chem., 114 (1925) 179.
60 H. W. B. Roozeboom in "Die heterogenen Gleichgewichte vom Standpunkte der Phasenlehre", Vieweg und Sohn, Braunschweig 1928, Vol. II, Part 2, p. 191.
61 S. L. Miller, E. I. Eger and C. Lundgreen, Nature, 221 (1969) 468.
62 O. L. Roberts, E. R. Brownscombe, L. S. Howe and H. Ramser, Petr. Eng., 12 (1941) 56.
63 W. M. Deaton and E. M. Frost, Oil Gas J., 36 (1937) 75.
64 W. M. Deaton and E. M. Frost, Gas 14 (1938) 31.
65 W. L. Wilcox, D. B. Carson and D. L. Katz, Ind. Eng. Chem., 33 (1941) 662.
66 B. Miller and E. R. Strong, Am. Gas Ass. Monthly, 28 (1946) 63.
67 P. Villard and R. de Forcrand, Compt. Rend., 106 (1888) 849, 1357.

68 D. N. Glew and M. L. Haggett, Can. J. Chem., 46 (1968) 3857, 3867.
69 D. N. Glew and N. S. Rath, J. Chem. Phys., 44 (1966) 1710.
70 O. Maass and E. H. Boomer, J. Am. Chem. Soc., 44 (1922) 1709.
71 D. G. Leaist, J. J. Murray, M. L. Post and D. W. Davidson, J. Phys. Chem., 86 (1982) 4175.
72 G. N. Werezak, Chem. Eng. Progr. Symp. Ser., 65 (1969) 6.
73 J. N. Wickert, W. S. Tamplin and R. L. Shank, Chem. Eng. Prog. Symp. Ser., 48 (1952) 92.
74 Y. P. Handa, J. Chem. Thermodyn., 17 (1985) 201.
75 L. Carbonnel and J.-C. Rosso, J. Solid State Chem., 8 (1973) 304.
76 J. Erva, Suomen Kemistilehti, 29B (1956) 183.
77 G. Meyer, J. W. White and H. J. M. Hanley, Abstr. 10th Symposium on Thermophysical Properties, NBS Maryland USA, 1988 June.
78 Y. P. Handa, J. Chem. Thermodyn., 16 (1984) 623.
79 R. E. Hawkins and D. W. Davidson, J. Phys. Chem., 70 (1966) 1889.
80 B. Morris and D. W. Davidson, Can. J. Chem., 49 (1971) 1243.
81 A. Venkateswaran, J. R. Easterfield and D. W. Davidson, Can. J. Chem., 45 (1967) 884.
82 K. W. Morcom and R. W. Smith, J. Chem. Thermodyn., 3 (1971) 507.
83 J.-C. Rosso and L. Carbonnel, Compt. Rend. Acad. Sci. Paris, 272 (1971) 136, 713.
84 J.-C. Rosso and L. Carbonnel. Compt. Rend. Acad. Sci. Paris, 272c (1971) 136. 713.
85 G. J. Wilson and D. W. Davidson, Can. J. Chem., 41 (1963) 264.
86 H. Nakayama and M. Tahara, Bull. Chem. Soc. Jpn, 46 (1973) 2965.
87 J. Kaloustian, J.-C. Rosso and L. Carbonnel, Compt. Rend. Acad. Sci. Paris, 275C (1972) 249.
88 L. Carbonnel, J.-C. Rosso and J. Kaloustian, Compt. Rend. Acad. Sci. Paris, 279C (1974) 241.
89 Y. P. Handa, J. Chem. Thermodyn., 18 (1986) 891.
90 Y. P. Handa, J. Chem. Thermodyn., 18 (1986) 915.
91 L. Aaldijk, Ph. D. Thesis, Technical Univ. Delft (1971).
92 G. J. Ewing, L. G. Ionescu, J. Chem. Eng. Data, 19 (1974) 367.
93 J. L. de Roo, C. J. Peters, R. N. Lichtenthaler and G. A. M. Diepen, AIChE J., 29 (1983) 651.
94 W. M. Deaton and E. M. Frost, U.S. Bureau of Mines Monograph No. 8 (1946).
95 H. O. McLoad and J. M. Campbell, J. Petr. Technol., 222 (1961) 590.
96 E. M. Frost and W. N. Deaton, Oil Gas J., 45 (1946) 170.
97 G. D. Holder and G. C. Grigoriou, J. Chem. Thermodyn., 12 (1980) 1093.
98 G. D. Holder and V. A. Kamath, J. Chem. Thermodyn., 14 (1982) 1119.
99 G. D. Holder and S. P. Godbole, AIChE J., 28 (1982) 930.
100 B. Miller and E. R. Strong, Jr., Proc. Am. Gas Assoc., 27 (1945) 80.
101 S. R. Gough and D. W. Davidson, Can. J. Chem., 49 (1971) 2691.
102 Y. P. Handa, J. Phys. Chem., 90 (1986) 5497.
103 A. van Cleeff, Dissert., Tech.-Hogeschool, Delft (1962).
104 D. N. Glew, J. Phys. Chem., 66 (1962) 605.
105 T. J. Galloway, W. Ruska, P. S. Chappelear and R. Kobayashi, Ind. Eng. Chem. Fundam., 9 (1970) 237.
106 G. H. Cady, J. Phys. Chem., 87 (1983) 4437.
107 W. G. Knox, M. Hess, G. E. Jones and H. B. Smith, Chem. Eng. Progr., 57 (1961) 66.
108 P. J. Ceccotti, I & EC Fundam., 5 (1966) 106.
109 N. G. Parsonage and L. A. K. Staveley, "Disorder in Crystals", Clarendon Press, Oxford (1978), Chap. 11.
110 J. H. van der Waals, Disc., Faraday Soc., 15 (1953) 261.
111 J. H. van de Waals, Trans. Faraday Soc., 52 (1956) 184.
112 J. H. van der Waals and Plateeuw, "Clathrate Solutions", Adv. Chem. Phys., Vol. 2, p. 1 (1959).
113 G. C. Maitland, M. Rigby, E. B. Smith and W. A. Wakeham, "Intermolecular Forces—

Their Origin and Determination", Clarendon Press, Oxford 1981.
114 T. Kihara, Adv. Chem. Phys., 9 (1963) 147.
115 Y. P. Handa and J. S. Tse, J. Phys. Chem., 90 (1986) 5917.
116 S. P. Barakov, A. Z. Savvin, V. P. Tsarev, Russ. J. Phys. Chem., 59 (1985) 608.
117 P. B. Dharmawardhana, W. R. Parrish and E. D. Sloan, Ind. Eng. Chem. Fundam., 19 (1980) 410.
118 D. W. Davidson, Y. P. Handa and J. A. Ripmeester, J. Phys. Chem., 90 (1986) 6549.
119 W. R. Parish and J. M. Prausnitz, Ind. Eng. Chem. Process Des. Dev., 11 (1972) 26.
120 D. W. Davidson, Y. P. Handa, C. I. Ratcliffe, J. S. Tse and B. M. Powell, Nature, 311 (1984) 142.
121 J. O. Hirschfelder, C. F. Curtiss and R. B. Bird, "Molecular Theory of Gases and Liquids", Wiley, New York 1954.
122 M. A. White and M. T. MacLean, J. Phys. Chem., 89 (1985) 1380.
123 J. Comper, A. Quesnel, C. A. Fyfe and R. K. Boyd, Can. J. Chem., 61 (1983) 92.
124 Y. P. Handa, Can. J. Chem., 63 (1985) 68.
125 O. Yamamuro, M. Oguni, T. Matsuo and H. Suga, Bull. Chem. Soc. Jpn, 60 (1987) 1269.
126 O. Haida, T. Matsuo, H. Suga and S. Seki, J. Chem. Thermodyn., 6 (1974) 815.
127 G. A. Neece and J. C. Poirier, J. Chem. Phys., 43 (1965) 4282.
128 J. C. Burgiel, H. Meyer and P. L. Richards, J. Chem. Phys., 43 (1965) 4291.
129 J. S. Tse, J. Phys. (Paris), Colloq., C1, 3 (1987) 543.
130 J. S. Tse, W. R. McKinnon and M. Marchi, J. Phys. Chem., 91 (1987) 4188.
131 O. Yamamuro, M. Oguni, T. Matsuo and H. Suga, J. Phys. Chem. Solids, 48 (1987) 935.
132 H. Suga and S. Seki, J. Non-crystl. Solids, 16 (1974) 171.
133 H. Suga and S. Seki, Faraday Discuss. No. 69, 221, Roy. Soc. Chem., (1981).
134 S. K. Garg, B. Morris and D. W. Davidson, J. Chem. Soc. Faraday Trans., II 68 (1972) 481.
135 S. R. Gough, E. Whalley and D. W. Davidson, Can. J. Chem., 46 (1968) 1673.
136 S. K. Garg, Y. A. Majid, J. A. Ripmeester and D. W. Davidson, Mol. Phys., 33 (1977) 729.
137 H. Suga, J. Chim. Phys. Phys-Chim. Biol., 82 (1985) 275.
138 N. Bjerrum, Science, 115 (1952) 385.
139 Y. Tajima, T. Matsuo and H. Suga, Nature, 299 (1982) 810.
140 Y. Tajima, T. Matsuo and H. Suga, J. Phys. Chem. Solids, 45 (1984) 1135.
141 A. J. Leadbetter, R. C. Ward, J. W. Clark, P. A. Tucker, T. Matsuo and H. Suga, J. Chem. Phys., 82 (1985) 424.
142 T. Matsuo, Y. Tajima and H. Suga, J. Phys. Chem. Solids, 47 (1986) 165.
143 M. Oguni, N. Okamoto, O. Yamamuro, T. Matsuo and H. Suga, Thermochim. Acta, 121 (1987) 323.
144 O. Yamamuro, T. Matsuo and H. Suga, J. Incl. Phenom., in press.
145 L. Pauling, J. Am. Chem. Soc., 57 (1935) 2680.
146 S. R. Gough, S. K. Garg and D. W. Davidson, Chem. Phys., 3 (1974) 239.
147 D. W. Davidson, Can. J. Chem., 49 (1971) 1224.

Zusammenfassung — Ausgehend von 147 Literaturangaben wurden in diesem Review thermodynamische Untersuchungen von Klathrathydraten hauptsächlich der Struktur I und II betrachtet. Es gibt zwei Hauptaugenmerke. Als erstes die Wirtsgitterenergie und die Gast-Wirt-Wechselwirkungsenergie, beide bezogen auf die Dissoziationsenthalpie und die Bildungsenthalpie der Hydrate. Das zweite Hauptaugenmerk betrifft Orientierungs-Konditionierungserscheinungen sowohl in Wirt als auch Gast, wie in den Wärmekapazitäten bei niedrigen Temperaturen widergespiegelt wird. Auf der Basis jüngster experimenteller Ergebnisse wurde die klassische theoretische Betrachtung über die Bildung von Klathraten überprüft. Der Orientierung-Konditionierung wurde besonderer Nachdruck verliehen, da dies zweifellos eine entscheidende Rolle bei der Klärung der Natur der Klathrathydrate spielt.

Резюме — В представленном на основе 147 литературных ссылок обозрении рассмотрены термодинамические исследования клатратных гидратов со структурами I и II. Рассмотрены две главные темы. В первой рассмотрены энергия решетки «хозяина» и энергия взаимодействия «хозяин — Гость», связанные с энтальпией диссоциации и разложения гидратов. Вторая тема касается явления ориентационного упорядочения в решетках «хозяин» и «гость», что отражается в низкотемпературной теплоемкости. Классическая теоретическая обработка образования кластеров пересмотрена на основе недавних экспериментальных результатов. Особое ударение сделано на ориентационном упорядочении, так как этот вопрос несомненно является центральным при выяснении природы клатратных гидратов.